EVOLUTION OF RADIATION POWER PROFILES IN ASDEX H-MODE DISCHARGES

E. R. Müller, G. Janeschitz, P. Smeulders[+]

IPP III/112 February 1986

MAX-PLANCK-INSTITUT FÜR PLASMAPHYSIK

8046 GARCHING BEI MÜNCHEN

MAX-PLANCK-INSTITUT FÜR PLASMAPHYSIK

GARCHING BEI MÜNCHEN

EVOLUTION OF RADIATION POWER PROFILES IN ASDEX H-MODE DISCHARGES

E. R. Müller, G. Janeschitz, P. Smeulders[+]

IPP III/112 February 1986

[+]Now JET Joint Undertaking, Abingdon, England

Die nachstehende Arbeit wurde im Rahmen des Vertrages zwischen dem Max-Planck-Institut für Plasmaphysik und der Europäischen Atomgemeinschaft über die Zusammenarbeit auf dem Gebiete der Plasmaphysik durchgeführt.

IPP III/112 E R Müller
G Janeschitz
P Smeulders*

Evolution of Radiation Power Profiles in ASDEX H-Mode Discharges

Abstract

The paper compares radiation power profiles, energy exhaust and impurity radiation mechanisms of the two types of H-mode during neutral-injection heated divertor discharges in the tokamak ASDEX. The normal H-mode discharge that reaches a quasi-stationary state is characterized by moderate radiation power losses of the main plasma and by repetitive burst-like energy release from its outer half-radius zone into the divertor. In contrast, the burst-free variant of the H-mode shows superior energy and particle transport properties but becomes dominated by radiation power losses growing continuously up to 100% of the heating power input. The dynamic behaviour, ie the variation in time, of the iron concentration and the associated radiation power density at the plasma centre is hardly influenced by the kind of H-mode. But, if the concentration of metals with medium Z-value is raised to sufficiently high values in the burst-dominated H-mode plasma, eg by the accumulation of intrinsic iron, the burst-free (or burst-deficient) H-mode is triggered, which after a new accumulation period usually ends by a radiation collapse.

* JET Joint Undertaking, Abingdon OX14 3EA, UK

CONTENTS

		Page
1.	Introduction	3
2.	The ASDEX tokamak and diagnostics	4
3.	Energy expulsion into the divertor by burst activity	5
4.	Burst-dominated and burst-free H-mode discharges	6
5.	Radial profiles of radiation power emission	8
6.	Power losses at the plasma edge	11
7.	Radiation power losses and impurity concentration at the plasma centre	12
8.	Triggering of the burst-free H-mode by external impurity injection or internal impurity accumulation	14
9.	Poloidal asymmetries in the radiation distribution	15
10.	Summary	17
	References	20

1. INTRODUCTION

The H-mode [1] of neutral-injection (NI) heated divertor discharges in the tokamak ASDEX that, in contrast to the L-mode, restores the good confinement properties of ohmic discharges is usually characterized by highly repetitive energy and particle expulsion from the main plasma volume into the divertor chambers, the phenomenon of the so-called bursts. After it had been demonstrated that the power losses into the divertor are almost blocked during the quiescent time intervals between bursts [2], discharges with long-lasting burst-free periods were produced [3]. This second type of H-mode exhibits superior energy and particle transport properties [4] but develops excessive radiation power losses that terminate the H-mode. A limitation of β is observed in both kinds of H-mode [5] and it is suggested in this context that self-stabilisation of the plasma pressure profile demands an effective energy exhaust from the plasma edge either by burst activity or by higher radiation power losses. Previous papers [3, 4,6] underline the fact that impurity accumulation causes centrally peaked radiation power profiles during the burst-free H-mode; but they do not give attention to the burst-dominated H-mode. This altogether has stimulated a more detailed and comprehensive investigation of the radiation power behaviour in H-mode discharges which is presented in this paper.

Section 2 of this paper describes the experimental arrangement. Section 3 restates briefly the principal results concerning the time pattern and the amplitude of energy bursts into the divertor [2]. Section 4 introduces two discharges representative of both variants of H-mode. Section 5 treats the time evolution of the radial radiation power profiles during the two H-modes. Section 6 investigates whether enhanced radiation power and burst activity can actually replace each other as energy exhaust channels within the plasma edge zone. Sections 5 and 7 deal with the dependence of the local radiation power density as well as impurity concentration at the plasma centre on the

presence or absence of bursts. These sections also answer the question for the dominant radiation power sources in the plasma core. The study of the dynamic behaviour of the central plasma radiation shows a new way, presented in Section 8, of achieving the burst-free H-mode: its internal triggering by accumulation of intrinsic iron during the preceding burst-dominated H-phase. Section 9 discusses poloidal asymmetries in the radiation distribution. The paper is summarised in Section 10.

2. THE ASDEX TOKAMAK AND DIAGNOSTICS

ASDEX is a tokamak combining an axisymmetric poloidal divertor in double-null configuration with a near-circular shape of the interior magnetic flux surfaces (Fig.1). The neutral-injection heating system consists of two tangential beam lines in co-direction capable of delivering a total neutral-beam power of up to 3.4 MW (H°, 40 kV) or 4.3 MW (D°, 45 keV) for pulse lengths of up to 0.4 s. If not otherwise stated, we discuss ungettered discharges in deuterium. The radiation behaviour and the global power balance of the ohmically heated plasma [7] as well as the NI-heated one in the L-mode [2] are characterized by two main features: In comparison with metallic limiters, the use of the divertor roughly halves the volume-integrated radiation power losses of the main plasma to values of around 20% of the total heating power and reduces even more efficiently the metal content and thus the local radiation power density at the plasma centre. Secondly, bolometrically detected volume power losses of the high-density divertor plasma consisting mainly of low-energetic neutral particle emission dissipate the major fraction of the energy flow into the divertor chambers.

The spectrum-integrated radiation power losses of the plasma are measured by means of an absolutely calibrated 19-bolometer array with a time resolution between 1 and 10 ms. The metal resistor bolometers are of the type

reported in Ref.[8]. Bolometers cannot distinguish between neutral particle and electromagnetic radiation emission. In addition to the array, several individual bolometers with an uncollimated view in the poloidal plane are distributed around the toroidal circumference and monitor the volume-integrated power losses. The bolometrically detected power losses in both the main chamber and the two divertor chambers are assumed to be isotropic and uniform in the toroidal and poloidal direction. The method of extrapolating the power losses determined in front of one neutralizer plate to those of all four plates is described in Ref.[7].

The surface-integrated net power absorbed by the divertor neutralizer plates is calculated from its surface temperature evolution measured by the thermographic system [9]. An infrared camera records up to 2500 temperature profiles per second along the poloidal direction of the plate with a space resolution of 1.3 mm.

Figure 1 also shows the photodiode measuring the H_α-light emission from the divertor plasma.

3. ENERGY EXPULSION INTO THE DIVERTOR BY BURST ACTIVITY

In normal H-mode discharges the energy and particle outflow into the divertor chambers are modulated by large-amplitude bursts: Figs.2 and 3 illustrate this characteristic time behaviour of the H_α-light, of the bolometrically detected neutral particle and radiation power emission from the divertor plasma and of the thermographically determined power deposition onto the divertor neutralizer plates. The thermographic measurements, performed with highest time-resolution in the submillisecond range, reveal that during the quiescent intervals between bursts the energy exhaust of NI-heated plasmas into the divertor is dramatically reduced to the level of the ohmic discharge phase. The power released by individual bursts varies by almost one order of magnitude and depends on, for example,

the burst frequency. Typical bursts of a discharge with 3 MW heating power show pulse lengths of around 0.5 ms and power amplitudes of the order of 1 MW, which means that during each burst an energy amount equivalent to that contained in a plasma annulus with 40 cm radius and a thickness of several cm is expelled into the divertor. The thermographic energy flux profile broadens considerably at the burst and thus manifests the periodic degradation of the energy confinement of the plasma edge during the bursts.

The dynamics of a L→H transition from the viewpoint of global energy balance is presented in Fig.4. During the quasi-stationary L-phase, ie from about 50 ms after the start of neutral injection, the sum of the three power loss channels accounted for, the volume-integrated radiation power and neutral particle emission in both the main chamber (RAD) and the two divertor chambers (RAD_{DIV}) and the surface-integrated power deposition onto the four divertor neutralizer plates (DEP), stays approximately constant though individual channels may show a pronounced variation with time. The spontaneous transition into the H-mode, the regime with improved energy confinement, is marked by a drop of all power losses and a simultaneous rise of the plasma energy content (β_p). When the blocking of the energy outflow across the separatrix into the divertor ends, ie RAD_{DIV} and DEP (both signals being time- averaged over the bursts) regain strength, the β_p signal saturates. During the last part of the H-phase the torus plasma radiation RAD intensifies and partly compensates the effect that the divertor power losses RAD_{DIV} and DEP keep below their L-mode levels. Nevertheless, the power accountability becomes worse in the H-mode.

4. BURST-DOMINATED AND BURST-FREE H-MODE DISCHARGES

H-mode discharges with prolonged NI-heating intervals and burst-free periods longer than 100 ms can be established reproducibly by a moderate outward shift of the plasma column. This makes it possible to investigate the influence

of the bursts on the long-term discharge behaviour, eg the achievement of an H-mode equilibrium, by contrasting this burst-free H-mode with the kind exhibiting the usual burst pattern. Fig.5 shows the time development of various plasma parameters for both types of H-discharges. They have identical parameter settings at the beginning of the NI-heating interval (I_p = 320 kA, B_t = 2.17 T, $\bar{n}_e$ = 3.5×10^{13} cm^{-3}, $P_{OH} + P_{NI}$ = 3.3 MW, $H^0 \rightarrow D^+$, NI from 1.1 s to 1.4 s), except for the major plasma radius which is R = 165 cm for the discharge with bursts and R = 169 cm for the burst-free one. Both discharges exhibit a brief L-phase during which not all signals become stationary. At t = 1.16 s a sharp decline of the H_α signal indicates the transition into the H-mode which results in an improved energy and particle content of the plasma (see the parameters τ_E^*, β_p, $\bar{n}_e$).

From the onset of clearly recognizable bursts at about 1.19 s this H-mode differs drastically from its burst-free variant. While with growing burst activity the power losses into the divertor time-averaged over the bursts (see RAD_{DIV} in Fig.6) recover from the temporary blocking, τ_E^*, β_p and $\bar{n}_e$ stop their increase, and may even decay if the β-limit has been approached [5], finally attaining stationary values which are above those of the L-mode. All radiation losses of the bulk plasma keep tolerably small.

In contrast, when the H-mode does not show any bursts during the entire course of time, the particle and the energy outflow into the divertor remain on a level as low as during the ohmic phase (see again RAD_{DIV} in Fig.6). The radiation power losses of the main plasma volume are considerably higher in the burst-free H-discharge than in the burst-dominated , even during the preceding L-phase (see RAD in Fig.6). This radiation enhancement indicates an impurity contamination of the plasma produced by its shift to the outer stainless-steel protection limiters. While the radiation power RAD continuously increases, accelerated by a simultaneous rise of the plasma density, the energy

replacement time τ_E^* as well as β_p pass through maxima comparable to those of the burst-dominated H-mode. The burst-free H-mode is terminated when the volume integrated main plasma radiation equalizes the total heating power input. Shortly prior to this radiation collapse, the local radiation power density of the plasma centre ($P_{RAD}(0)$) starts to grow exponentially up to tremendous values.

5. RADIAL PROFILES OF RADIATION POWER EMISSION

It has already been pointed out [3] that in the burst-free H-mode accumulation of metal impurities takes place yielding radial profiles of radiation power density that are peaked at the centre. This paper shows that metal impurities accumulate as well in the burst-dominated H-mode creating profiles of radiation power density likewise centrally peaked (Fig.7), although the absolute values of volume power emission are half an order of magnitude smaller.

The time evolution of the non-inverted chordal intensity profile of the 19-bolometer array for both types of H-mode gives a deeper insight into what happens. During the burst-dominated H-mode of shot #11338, the chord-intensity profile grows strongly within the inner half-radius from about t = 1.215 s and it becomes sharply peaked at the centre (Fig.8). After about 50 ms the development of the central radiation peak is turned into a decrease towards an equilibrium profile identical to that at t = 1.215 s. During the decay the profile runs through the same sequence of shapes but in the reverse direction. All the dramatic profile variations are restricted to the plasma core with radii up to 20 cm.

The elevated intensity recorded by the two edge bolometers, the sight-lines of which intersect the surrounding region of the upper stagnation point (see also Fig.1), can be attributed to locally enhanced radiation losses, quite in agreement with other indications of intense recycling in the proximity of the upper stagnation point.

During the alternative H-mode, represented by the burst-free phase of shot #11447, the chordal intensity profile of radiation power rises over its nearly entire radial range and this evolution to a profile peaked at the centre does not reach an equilibrium but continues for about 50 ms until the radiation collapse brings the H-mode to an end and leads back to the L-mode (Fig.9).

Fig.10 summarizes the Figures 8 and 9. Obviously, the burst activity does not prevent radiation profiles from becoming pronouncedly peaked at the centre but the repetitive burst-like release of plasma energy does on the time-average efficiently suppress any enlargement of radiation power within the outer plasma half-radius. The chordal intensity profile of the burst-dominated H-mode stays always, even during its transient central peaking, distinctly below the base profile from which the fatal radiation increase of the burst-free H-mode starts at t = 1.215 s.

The radial profiles of radiation power density $P_{RAD}(r)$ (Figs.11 and 12) obtained by Abel-inversion reflect, of course, the just listed crucial features of the non-inverted profiles. In Sec.9 we will see that Abel-inversion of chord-intensity profiles is a dubious undertaking for the burst-free H-mode. But even in the worst case, at the end of the burst-free H-phase, the radiation power density at the plasma centre $P_{RAD}(0)$ agrees with the value provided by two-dimensional soft x-ray tomography within a 35% accuracy limit.

The double-humped shape of the radiation power density profiles during both the L- and the initial H-phase (prior to t = 1.215 s) is specific to NI heating, ie it has never been observed during RF heating. This suggests that the radiation losses at small radii are considerably enhanced by charge exchange processes between impurity ions and beam neutrals (see Sec.7) shifting the impurity ionization equilibrium to a less ionized and more radiative distribution [10,11].

Spectroscopy and soft x-ray diagnostics confirm that the centre-peak development of the bolometric profile during both H-mode versions is dominantly due to increasing line radiation of highly ionized iron (Fig.5) and they exclude distortions of the bolometric chord-intensity measurements by Marfe-like [12] phenomena.

The central peaking of the radiation power profile during the burst-dominated H-mode is the result of an impurity accumulation, since Fig.13a shows that the changes of temperature as well as density do not exceed 10% for radii smaller than 20 cm in the time interval between 1.20 and 1.27 s ($T_e(0) \approx 2.3$ keV, $n_e(0) \approx 4.9 \times 10^{13}$ cm^{-3}). The impurity influx even decreases going from the L-mode to the H-mode [3]. The considerable rise of radiation power as well as plasma density ($n_e(o) = 5.4 \rightarrow 8.4 \times 10^{13}$ cm^{-3}) during the burst-free H-mode causes a drastic temperature drop ($T_e(o) = 1.5 \rightarrow 0.7$ keV), as can be seen in Fig.13b. Because of the negative temperature-coefficient of impurity line radiation, both the density and temperature variations contribute in accelerating the rapid growth of the centrally peaked radiation power profile. Nevertheless, the term impurity accumulation applies also to this type of H-mode: computer simulations have proved a strong inward convection to be essential for anomalous transport [3, 13]; Figures 9 and 12 reveal that between 1.245 s and 1.260 s the central radiation gains intensity at the cost of edge radiation.

The outward decline of the edge peak of the radiation power density profile of the burst-free H-mode (Fig.12) and the flat edge peak of the burst-dominated H-mode (Fig.11) form complements to the almost suppressed and the relatively high (time-integrated over the bursts), respectively, energy flow in the scrape-off layer.

6. POWER LOSSES AT THE PLASMA EDGE

In Figure 14 the radiation power density profiles for the two H-mode types are compared with the calculated profiles of the direct power input through the neutral beams to the electrons (P_e) and ions (P_i), respectively. The computations of P_e and P_i used the Monte-Carlo code FREYA [14], and it should be noted that the effective power input to the electrons is about twice as high as P_e because of the power transfer from the ions. The profiles are plotted vs r^2 that is proportional to the volume of the plasma column within radius r. During the burst-dominated H-mode those radiation power losses accumulating inside of 20 cm radius constitute always a small fraction of the volume-integrated radiation power and remain far below the electron power input. This implies that the transient central peaking of the radiation profile is not responsible for the β-limitation. There is more evidence confirming that statement: the β_p value does not recover from falling (Fig.5) when the radiation peak has passed its maximum and diminishes (Fig.8). Secondly, the β_p curve of this burst-dominated H-discharge reaches its maximum at about the same instant and the same amplitude as the burst-free counterpart (Fig.5), but with considerably lower central radiation power losses (Fig.10). Thirdly, shot #13096 gives a fine example, where β_p levels off clearly before the central radiation peak even starts to grow (Fig.15). To summarize, the similar time-behaviour of β_p and the radiation power density at the plasma centre during the burst-dominated H-phase, an increase and a subsequent decrease, has no causal connection but seems to have a common origin in the improved energy and (impurity) particle confinement both linked together.

The saturation of the plasma energy content (β_p) in all analyzed discharges of this kind is connected rather with the plasma edge located burst activity and the associated energy flow into the divertor than with the power losses at the plasma centre. This is understood by considering that large contributions to the global quantity β_p are provided by the

plasma volume at intermediate radii between 20 cm and 30 cm. The burst activity affecting the plasma from the edge as far as 20 cm radius (Fig.10) thus withdraws substantial energy from this zone by expulsion into the divertor.

In the burst-free H-mode, the main plasma radiation (RAD) becomes the dominant energy loss channel. Therefore, the energy flow into the divertor (see RAD_{DIV} signal in Fig.6) remains low and does not restore the previous L-mode level as one would expect for transport-dominated losses after the plasma equilibrium (with improved confinement) is re-established. When β_p saturates at t = 1.23 s, the huge edge peak still predominates the radiation power losses (Fig.14); the final exponential growth of the central radiation peak has not yet begun (Fig.16). The enlarged radiation from the outer plasma half-radius acts in this H-mode type as a substitute power loss channel for the extinguished burst activity:

Both the burst activity in the burst-dominated H-mode and the gain in edge radiation power in the burst-free H-mode have the same energy exhaust capability, which is of the order of MW (see Sec.3).

Both energy depletion mechanisms are effective within the same radial range between 20 and 40 cm (see Sec.5).

During the course of time the central peak of the radiation profile assumes more and more importance and contributes a significant fraction of the radiation power losses (Fig.12).

7. RADIATION POWER LOSSES AND IMPURITY CONCENTRATION AT THE PLASMA CENTRE

The question remains, what influence do the bursts exert on the behaviour of the plasma core. Figure 16 displays the time history of the local radiation power density at the plasma centre ($P_{RAD}(0)$) for the two H-discharge variants.

The logarithmic $P_{RAD}(0)$-scale makes it easier to separate the variation in time from the absolute magnitude. The essential result is that the time dependence of $P_{PAD}(0)$, particularly the time-constant of the exponential rise after the L-to-H mode conversion, is scarcely influenced by the type of H-mode. But the $P_{RAD}(0)$-vs-time curve of the burst-free H-discharge, including the transit phase of the L-mode, has about 3 times higher absolute values of $P_{RAD}(0)$ at any instant compared with the burst-dominated. This makes it evident that the development of extremely high radiation power losses at the plasma centre in burst-free H-discharges is not due to an increase at a particularly dreadful rate but due to the already initially larger iron contamination.

In order to correct for the large density and temperature variations in the burst-free H-mode (Fig.13) and to get a quantity that is proportional to the metal impurity concentration, $P_{RAD}(0)$ is divided by both the central density squared $n_e^2(o)$ and the temperature-dependent radiative power loss function of iron $P_{Fe}(T_e)$ [10,11]. It is assumed that iron exclusively causes the radiation power losses at the plasma centre. We use those radiation loss calculations which include charge exchange with beam neutrals as a recombination mechanism shifting the ionization equilibrium. We take $n_o/n_e = 10^{-5}$ as the toroidal average of the non-uniform distribution of beam neutrals seen by the iron ion as it moves rapidly around the torus following the magnetic field lines. At plasma temperatures above 1 keV this ratio of n_o/n_e yields an enlargement of iron radiation power by almost one order of magnitude.

Interpreting Fig.17, which presents the result, one must be aware of the relatively large uncertainties. After the spontaneous L→H mode transition the calculated iron concentration at the plasma centre responds with a considerable time delay of more than 50 ms (compare Ref.[4]). In both kinds of H-mode the concentrations rise at rates very close to exponential with time-constants around 50 ms, that being roughly twice as long as during the preceding L-phase, up to

levels between 2 and 3 times higher than in the corresponding L-phase. The extraordinarily high iron concentration of the order of 1% at the end of the burst-free H-mode agrees with that derived from spectroscopic data by means of one-dimensional transport code calculations [13].

To summarize, the burst activity has a negligible influence on the time-dependent terms of the iron concentration evolution at the plasma centre. Just the other way round, if the time-independent term of the iron concentration, ie the value at the beginning of the NI interval, is sufficiently high then the bursts do not occur.

8. TRIGGERING OF THE BURST-FREE H-MODE BY EXTERNAL IMPURITY INJECTION OR INTERNAL IMPURITY ACCUMULATION

The hypothesis that a sufficiently high degree of plasma contamination with components of stainless-steel is needed to establish the burst-free H-mode has been verified experimentally by deliberate and controlled impurity injection into the plasma. Various impurities were injected either by gas puffing (neon, methane, argon) or by laser ablation (aluminium, chromium). Chromium, like iron a metal with medium Z-value, is the only injected material found capable of converting an H-mode with sporadic bursts into an absolutely burst-free one with all the properties discussed above (Fig.18). Figure 18 brings out again that the edge localized radiation reacts instantly to the disappearance and recurrence of the bursts whereas the radiation losses in the plasma centre follow with a large delay.

After we have seen that the long-lasting burst-free H-mode can be achieved by the activation of an external source of medium-heavy metal impurities, the issue remains whether the accumulation of intrinsic impurities during the burst-dominated H-mode is able to trigger internally the burst-free mode. Shot #12218 (Figs.19 and 20) proves that

the burst-dominated H-mode with initially moderate radiation power losses may well turn by itself into a burst-deficient mode with disastrous radiation consequences. The mode conversion occurs when the impurity accumulation process during the burst-dominated H-phase has raised the central radiation chord-intensity that indicates the local iron concentration up to the threshold value of the burst-deficient H-mode (Fig.20). The first and the last step in the radiation profile evolution show a striking resemblance to their burst-dominated and burst-free counterparts during the shots #11338 and #11447, respectively (Figs.8 and 9). The burst-dominated H-mode of shot #11338 seems not to convert, because the central peak of its radiation chord-intensity profile does not touch the base profile of the corresponding burst-free H-mode (Fig.10).

Figures 18 and 19/20 demonstrate that frequently the change in the type of H-mode is much more clearly recognizable from the time behaviour of the radiation power profile than from the burst activity of the H_α-light. Therefore, the more generalized terms Edge-Localized-Mode(ELM)-dominated and ELM-free H-mode [3] are more suitable for the H-mode classification.

9. POLOIDAL ASYMMETRIES IN THE RADIATION DISTRIBUTION

The constancy of the centre-chord intensity during the transition from the burst-dominated to the burst-deficient H-phase (Fig.20) is without any apparent cause. There are two possible explanations: 1. This event is accidental and Abel-inversion can be carried out without constraints yielding radiation power density profiles with a gain in edge peak height at the expense of a reduced central peak.
2. The distribution of radiation power density along the central chord actually does not change and the increment in the off-centre chordal intensities is due to a local enhancement of radiation power above as well as below the plasma centre.

The second argument is supported by another result. Figure 21 compares the total radiation power obtained by volume-integration of the Abel-inverted bolometer array data with that measured directly by an individual bolometer with uncollimated view in the poloidal plane. The agreement is excellent for the ohmic, the L-phase and the burst-dominated H-mode. During the burst-free H-mode we observe a discrepancy becoming continuously larger until the recurrence of the L-mode re-establishes the agreement. Since the uncollimated bolometer accounts for almost one hundred per cent of the total heating power at the end of the burst-free H-phase it obviously gives the correct result, whereas the array measurement with subsequent Abel-inversion and volume-integration yields too high values. Breaking up the volume integral into six discrete radial components (Fig.22) reveals that the radiation emission that leads to the overestimation is located initially at the plasma edge but then moves towards medium and small radii. Since the array and the uncollimated bolometer are mounted at the same flange with identical visual fields, the outward shift of the magnetic flux surfaces due to finite-beta effects cannot be responsible, particularly if one remembers that β covers the same range in both H-mode types, but the problem arises only in the burst-free mode. The unreliably high volume-integral of radiation power losses fits the second explanation of the phenomenon reported at the beginning of this Section and this confirms the idea that during the burst-free H-mode the contours of constant radiation emissivity evolve towards shapes deviating from circular symmetry that is a fundamental assumption for Abel-inversion.

Our interpretation agrees qualitatively with experimental results of the two-dimensional soft x-ray tomography that detects banana-like structures as well as top and bottom shoulders in the soft x-ray emission pattern during the burst-free H-mode (Ref.[6] and Fig.23). These poloidal asymmetries in the soft x-ray emissivity contract also towards the centre in the course of time, and they almost vanish as soon as bursts occur.

Theoretical estimates [15] suggest that the burst-dominated and burst-free H-mode are associated with different toroidal rotation velocities of the plasma. In this model the poloidal asymmetries of radiation power distribution are connected with a redistribution of impurities in the poloidal plane caused by the changed centrifugal force term in the momentum equation.

10. SUMMARY

Radiation power profiles, energy exhaust and impurity radiation mechanisms have been investigated for the two types of H-mode during neutral-injection heated divertor discharges in ASDEX. During each kind of H-mode the radial radiation power profiles evolve towards centrally peaked shapes. During the normal H-mode the highly repetitive burst-like expulsion of plasma energy into the divertor due to the Edge Localized Modes (ELMs) prevents any long-term increase of radiation power at plasma radii between a/2 and a. In this case, the growth of the central radiation power peak is restricted to the inner plasma half-radius and, finally, an equilibrium profile is achieved. The volume-integrated radiation power losses of the main plasma usually keep below 30% of the total heating power. In contrast, during the long-lasting burst-free version of the H-mode, where the energy outflow into the divertor is permanently reduced to its ohmic level, the radiation power losses grow unimpeded over nearly the whole plasma cross-section and become the major energy loss channel. The burst-free H-mode collapses when the volume-integrated radiation power losses approach the total heating power. Depending on the class of H-mode, the burst activity or the enhanced radiation power provide the essential energy loss mechanism within the outer plasma half-radius.

In agreement with VUV-spectroscopy and absolutely calibrated soft X-ray diagnostics, the radiation power peak at the

plasma centre can be attributed dominantly to line radiation of highly ionized iron that is shifted to an even more radiative ionization equilibrium by charge-exchange recombination with beam neutrals. The central peaking of the radiation power profiles reflects an impurity accumulation taking place irrespective of the H-mode type. The variation in time of the local radiation power density $P_{RAD}(o)$ as well as iron concentration at the plasma centre, particularly the time-constant of their exponential rise after the L-to-H mode conversion, is hardly influenced by the presence or absence of bursts. The absolute magnitude of $P_{RAD}(0)$, however, is at any instant, including the preceding L-phase, about three times higher in the burst-free H-mode as compared with the burst-dominated one, due to the already initially enlarged iron contamination. At the end of the burst-free H-mode, the radiation power density and the iron concentration at the plasma centre attain values of the order of several $W \cdot cm^{-3}$ and one per cent, respectively.

Vice versa, a sufficiently high degree of plasma contamination with medium-heavy metals is required to establish the long-lasting burst-free H-mode. This mode can be triggered externally either by a plasma shift towards the outer stainless-steel protection limiters or by deliberate laser ablation of metals with medium Z-value. But the conversion into the burst-free H-mode, that develops excessive radiation power losses, can also be triggered internally if the accumulation of intrinsic iron during the preceding burst-dominated H-phase is sufficiently strong. We have observed a pronounced threshold level of the central radiation chord-intensity associated with the local iron concentration. The transition from the burst-dominated into the burst-free H-mode is accompanied by growing locally enhanced radiation power losses. These poloidal asymmetries cause considerable deviations of the contours of constant radiation emissivity from circular symmetry and from magnetic flux surfaces, also at medium and small radii.

ACKNOWLEDGEMENTS

The authors acknowledge the continuous support of the whole ASDEX team, the NI team and the ASDEX Data Acquisition Group. Particularly, they wish to express their thanks to G Fussmann, O Gruber and M Kornherr for fruitful discussions and making their data available. They are grateful to G v Gierke, M Keilhacker and F Wagner for encouragement and support. Thanks are also due to H Wolf for technical assistance, to H Volkenandt for preparing the drawings and to C Simmons for handling the secretarial work.

REFERENCES

[1] Wagner F. et al., Phys.Rev.Lett. 49 (1982) 1408.

[2] Müller E R, et al., Journ.Nucl.Mat. 121 (1984) 138.

[3] Keilhacker M, et al., in Plasma Physics and Controlled Nuclear Fusion Research (Proc. 10th Int.Conf. London, 1984) Vol.1, IAEA, Vienna (1985) 71.

[4] Gruber O, Jilge W, et al., in Controlled Fusion and Plasma Physics (Proc.12th Europ.Conf. Budapest, 1985) Europhys. Conf. Abstr. Vol.9F Part I (1986) 18.

[5] Gierke G v, et al., in Controlled Fusion and Plasma Physics (Proc. 12th Europ.Conf.Budapest, 1985) Europhys. Conf. Abstr. Vol.9F Part I (1986) 331.

[6] Smeulders P, Nucl. Fus. 26 (1986) 267

[7] Müller E R, Behringer K, Niedermeyer H, Nucl.Fus. 22 (1982) 1651.

[8] Müller E R, Mast F, J.Appl.Phys. 55 (1984) 2635.

[9] Müller E R, Bein B K, Steinmetz K, Report IPP III/97, Garching (1984).

[10] Jensen R V, Post D E, Grasberger W H, Tarter C B, Lokke W A, Nucl.Fus. 17 (1977) 1187.

[11] Hulse R A, Post D E, Mikkelsen D R, J.Phys.B: Atom.Molec.Phys. 13 (1980) 3895.

[12] Niedermeyer H, et al., in Controlled Fusion and Plasma Physics (Proc. 12th Europ.Conf.Budapest, 1985) Europhys. Conf. Abstr. Vol.9F Part I (1986) 159.

[13] Fussmann G, Bartiromo R, Janeschitz G, Kotze P B, Müller E R, et al., in Controlled Fusion and Plasma Physics (Proc. 12th Europ.Conf.Budapest, 1985). Europhys. Conf. Abstr. Vol.9F Part I (1986) 195.

[14] Lister G G, et al., in Plasma Heating in Toroidal Devices (Proc. 3rd Int.Symp. Varenna, 1976) Editrice Compositori, Bologna (1976) 303.

[15] Feneberg W, Kornherr M, Smeulders P, in Controlled Fusion and Plasma Physics (Proc. 12th Europ.Conf. Budapest, 1985) Europhys. Conf. Abstr. Vol.9F Part I (1986) 299.

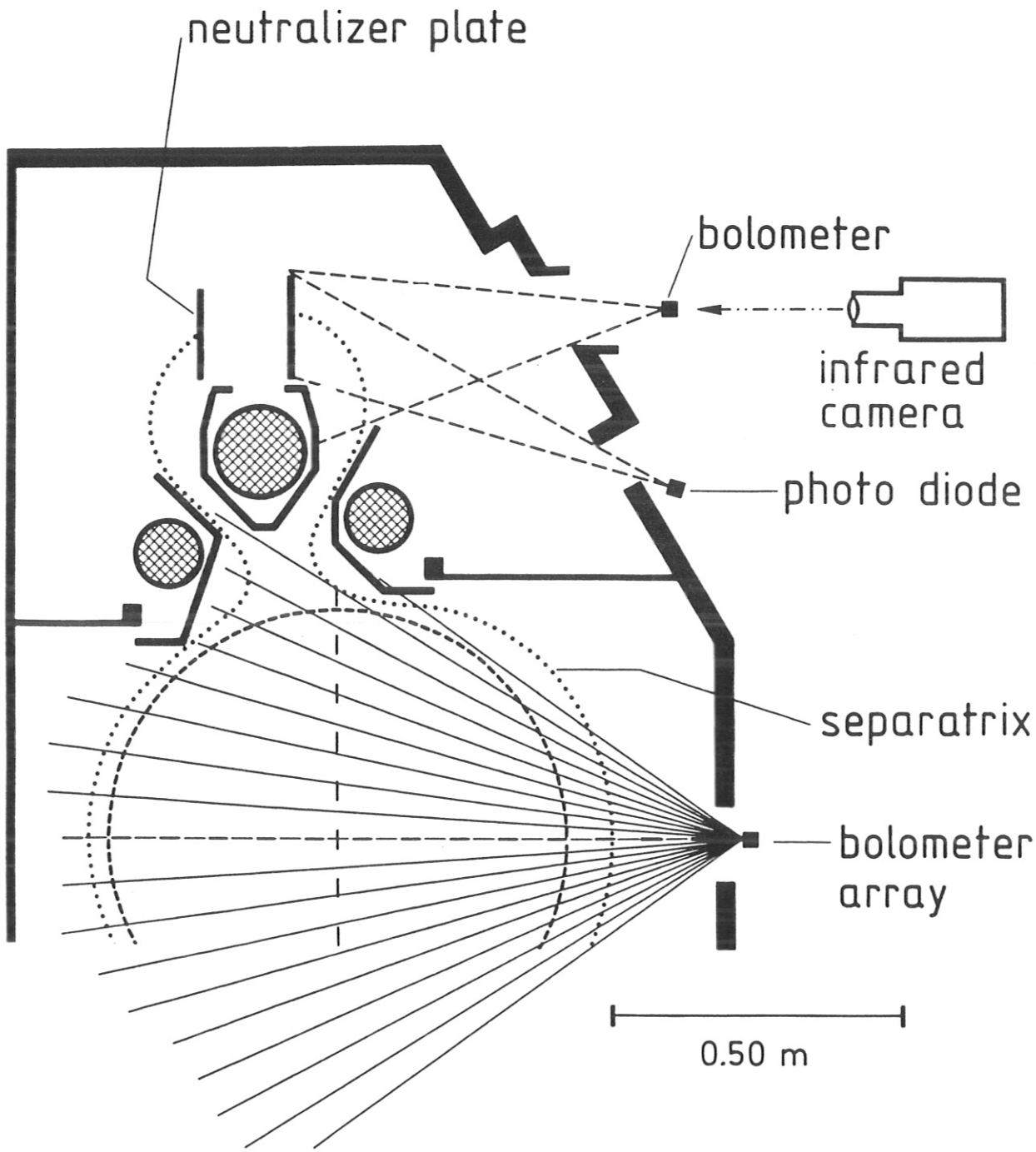

Fig.1 Cross-sectional view of the upper half of the ASDEX vessel with bolometer arrangement and lines of sight.

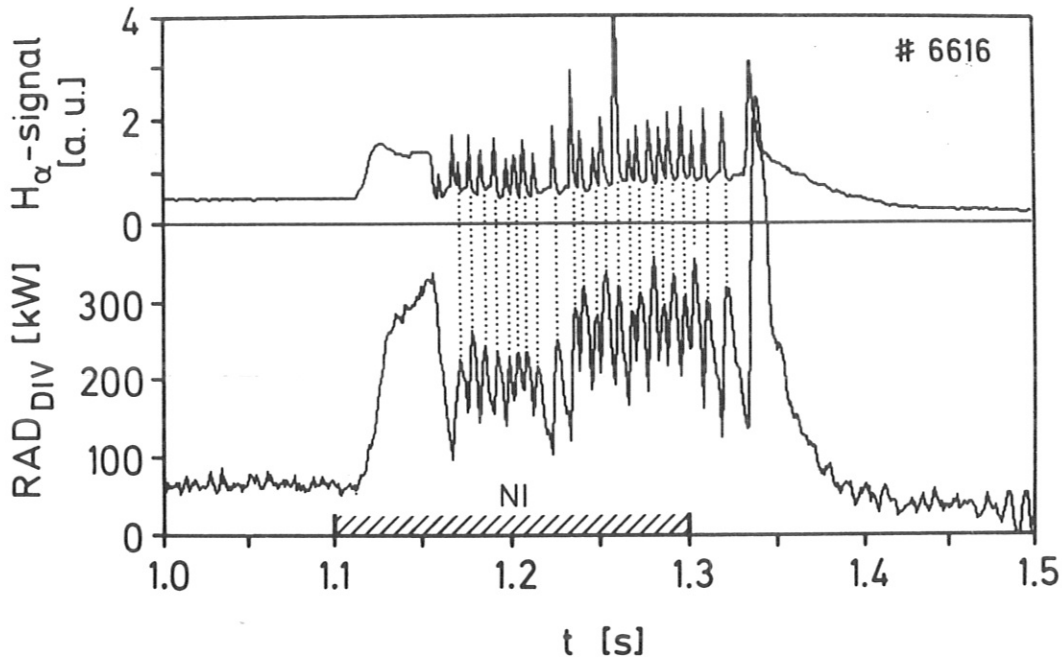

Fig.2 Time correlation of the H_α signal with the bolometrically recorded neutral particle and radiation power losses from the divertor plasma during an H-mode discharge with strong burst activity (I_p = 300 kA, $\bar{n}_e = 3.5 \times 10^{13}$ cm^{-3}, $P_{OH} + P_{NI} = 2.1$ MW).

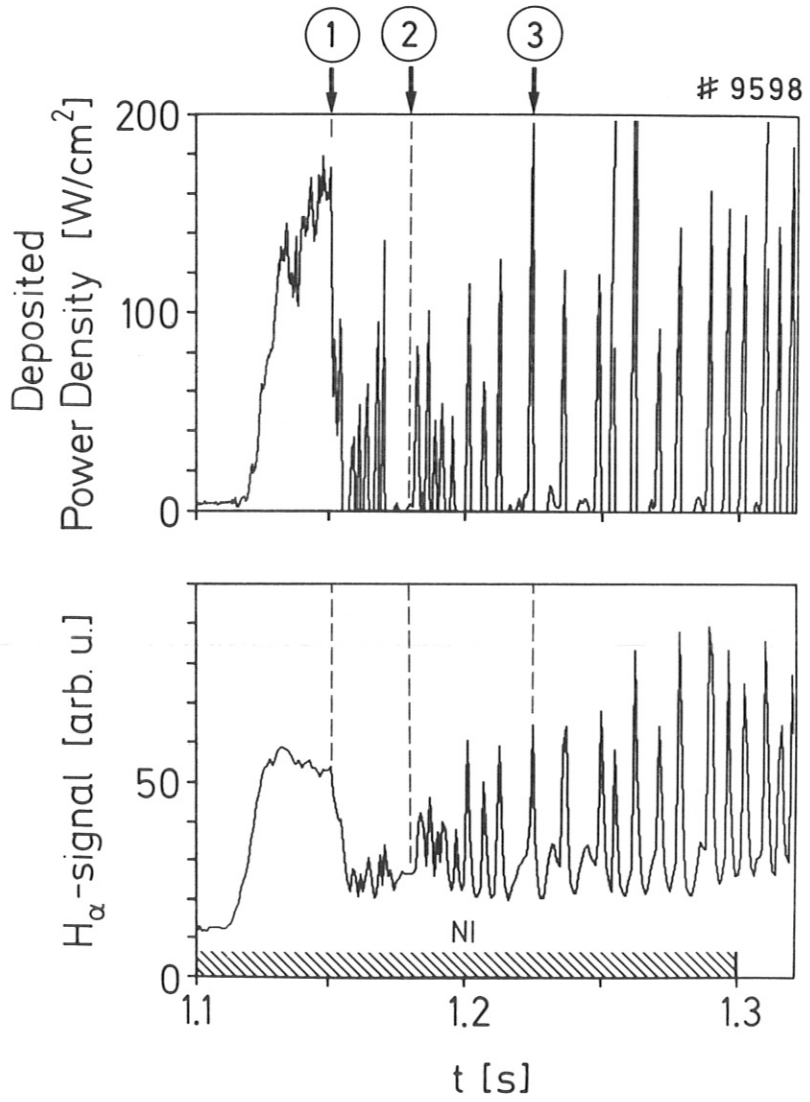

Fig.3 Variation in time of the power deposition density on the divertor neutralizer plates during different NI phases: (1) L-phase; (2) quiescent H-phase between bursts; (3) at burst maximum. For comparison, the H_α signal is shown (I_p = 320 kA, $\bar{n}_e = 4 \times 10^{13}$ cm^{-3}, P_{NI} = 2.85 MW).

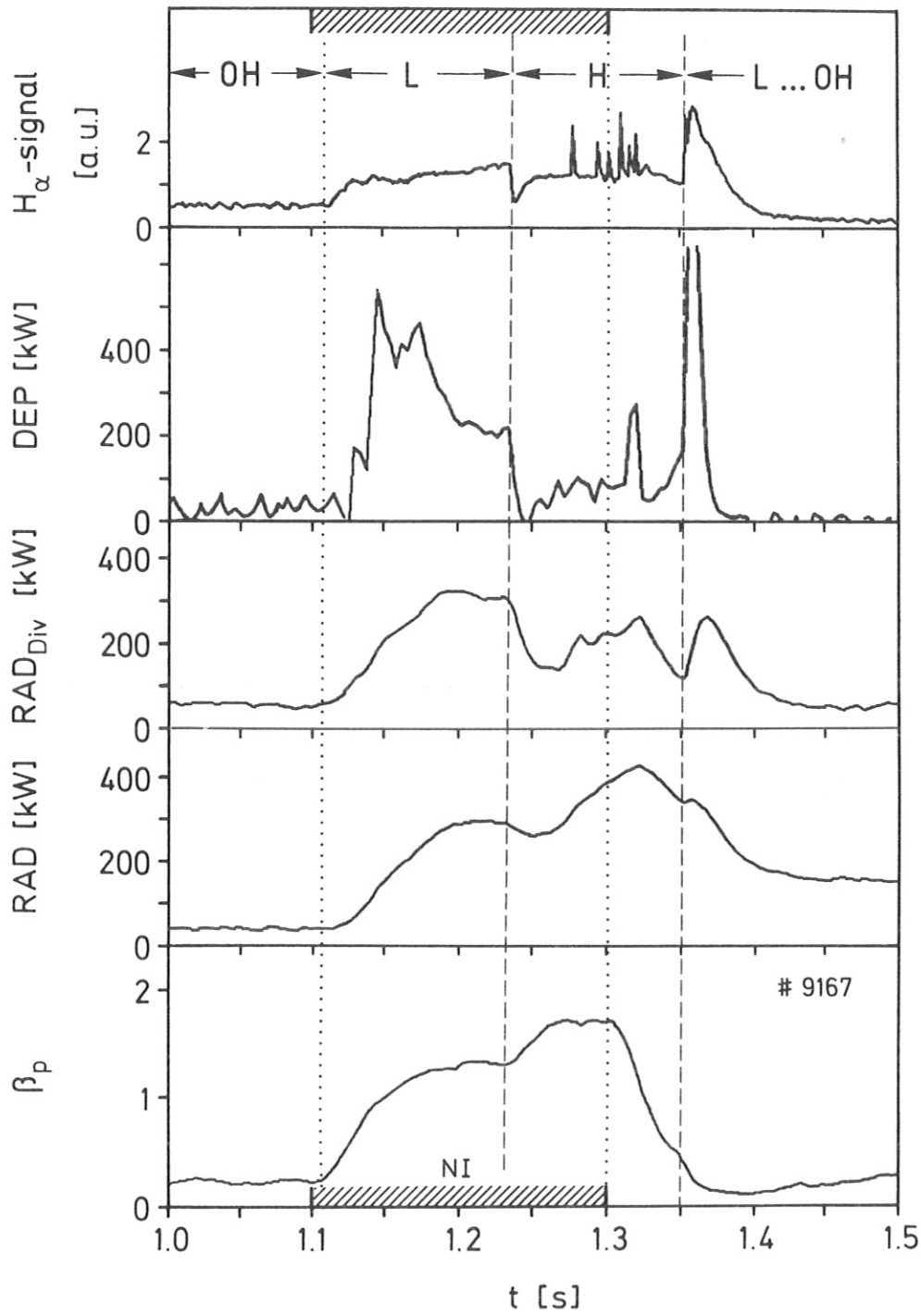

Fig.4 Time history of the global power balance during a L-H transition (I_p = 300 kA, $\bar{n}_e$ = 2.2x10^{13} cm^{-3}, P_{OH}+ P_{NI} = 2.1 MW. Both bolometric signals are smoothed by electronic time-constants of about 10 ms; for the analysis of the thermographic signal only each 10th of the 2500 temperature line profiles recorded per second is used).

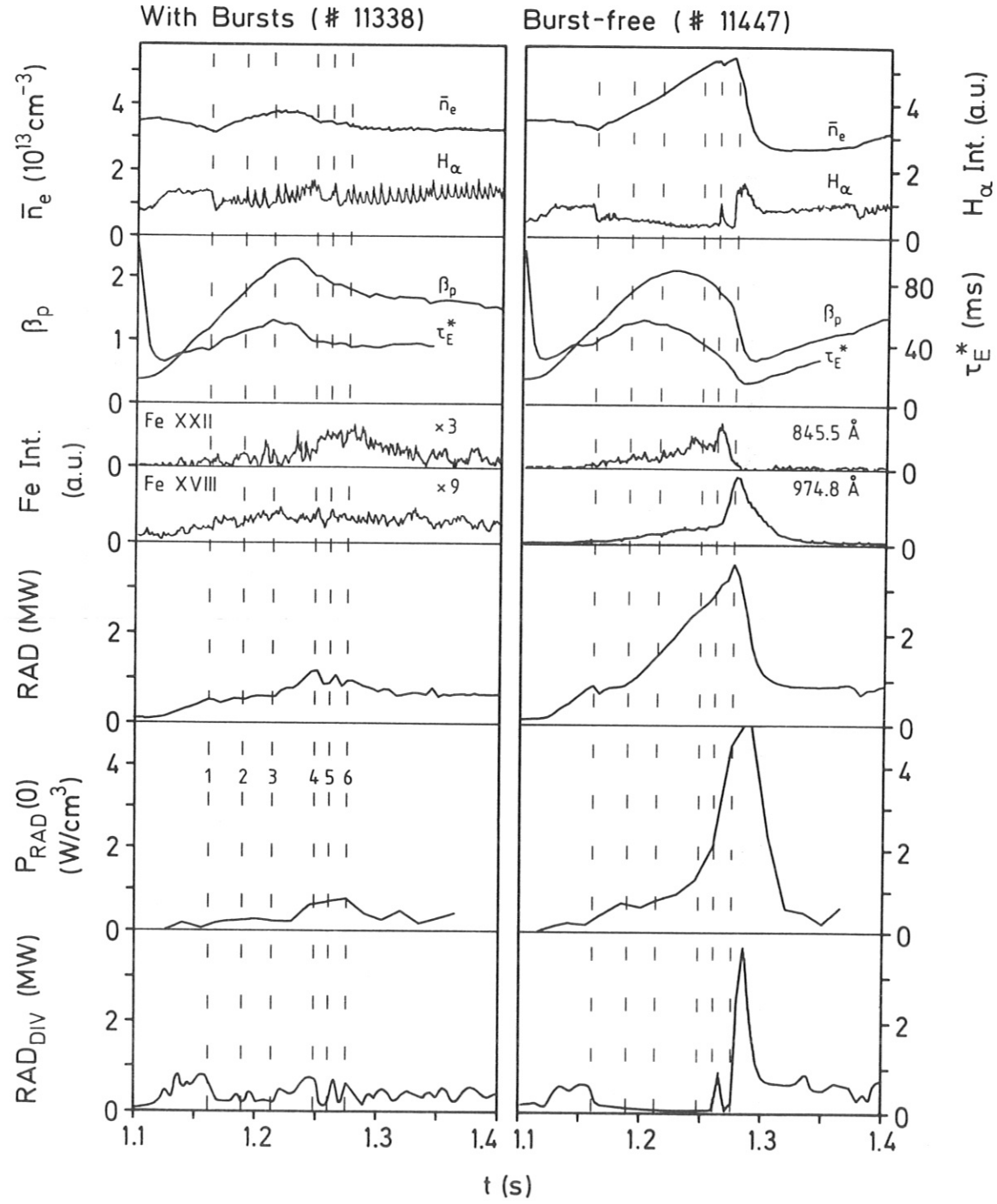

Fig.5

Time evolution of various plasma parameters during a burst-dominated (shot #11338) and a burst-free (shot #11447) H-discharge (I_p = 320 kA, B_t = 2.17 T, $\bar{n}_e$ (t=1.1 s) = 3.5x10^{13} cm^{-3}, P_{OH} + P_{NI} = 3.3 MW, $H^0 \rightarrow D^+$, NI from 1.1 s to 1.4s): the line-averaged plasma density $\bar{n}_e$, the H_α-light intensity, beta poloidal β_p, the global energy replacement time τ_E^*, the Fe XVIII and Fe XXII line intensities representative of iron radiation from r/a ≈ 2/3 and the centre, respectively, the volume-integrated radiation power and neutral particle losses in both the main chamber (RAD) and in the two divertor chambers (RAD_{DIV}), and the local radiation power density at the plasma centre ($P_{RAD}(0)$).

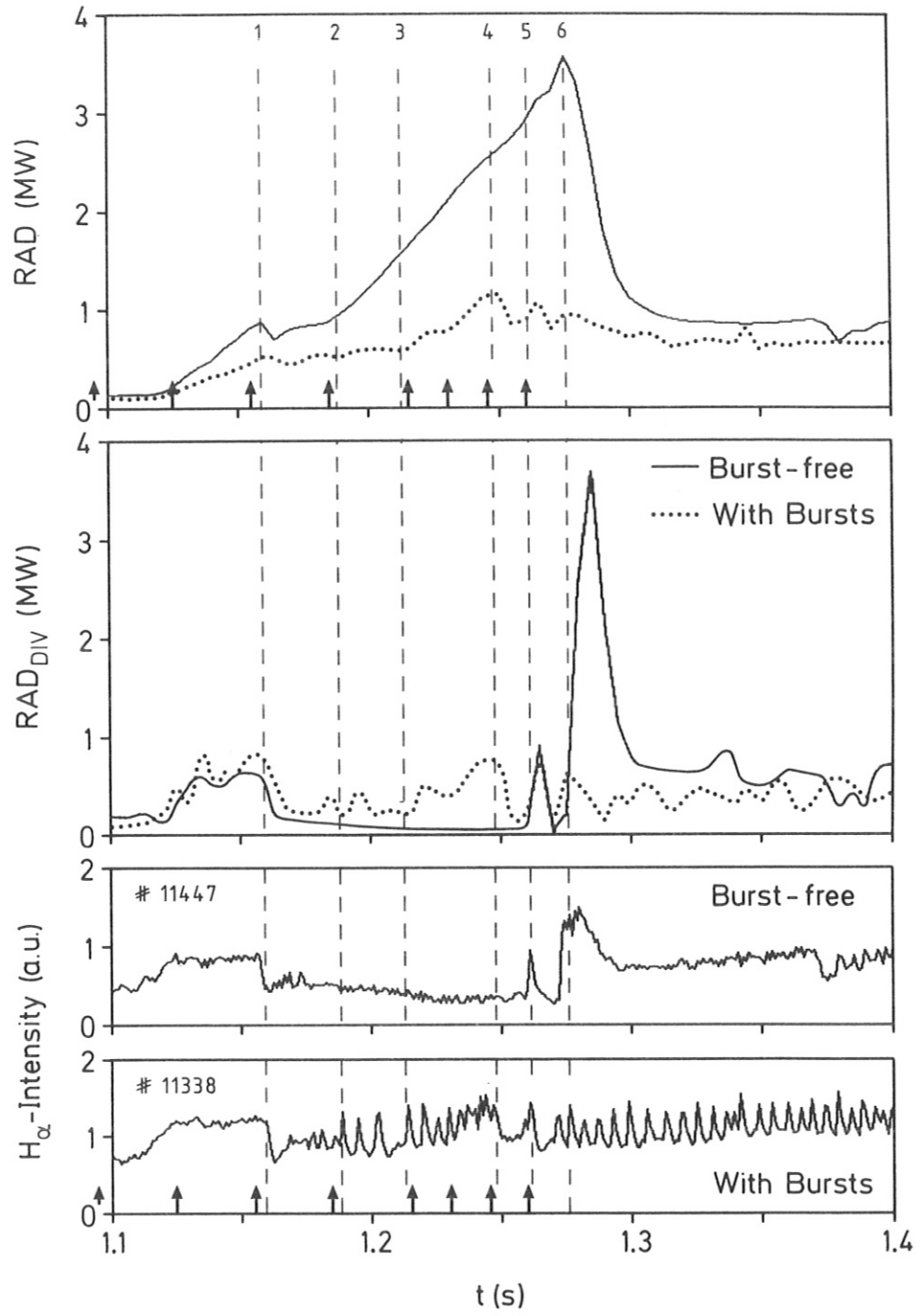

Fig.6

Time development of the volume-integrated radiation power and neutral particle losses in both the main chamber and in the two divertor chambers during the burst-free H-discharge in comparison with the burst-dominated one (blown-up presentation of part of Fig.5; the smoothing of the RAD_{DIV} signal is due to the electronic time-constant of about 10 ms; the arrows mark the times for which radiation profiles are presented in Figs.8 to 12).

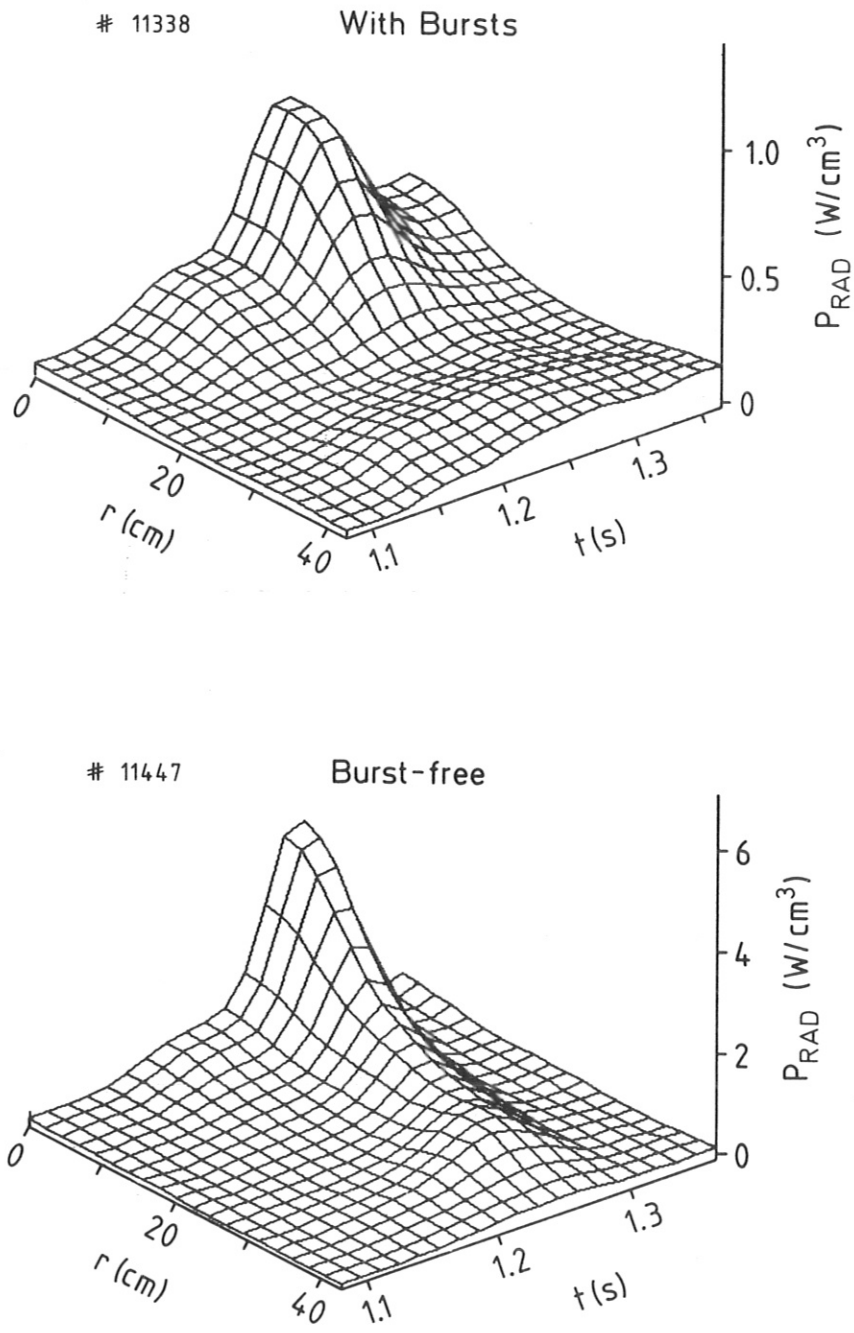

Fig.7 Evolution of the radial profiles of radiation power density towards centrally peaked shapes during both types of H-modes.

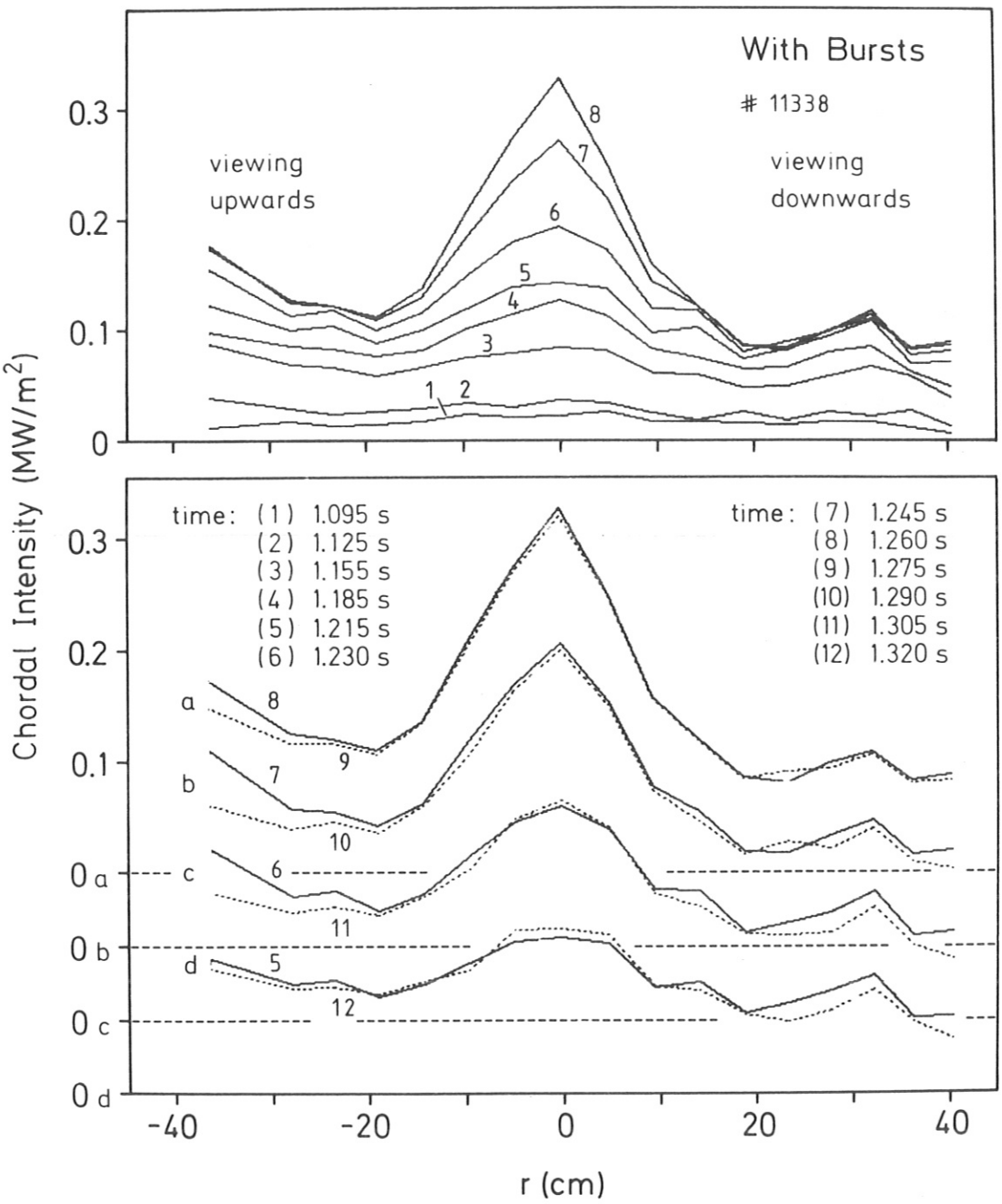

Fig.8 The increase (top) and decay (bottom) of the bolometric non-inverted chord-intensity profile during the burst-dominated H-mode, the profile running through the same sequence of shapes during reversion.

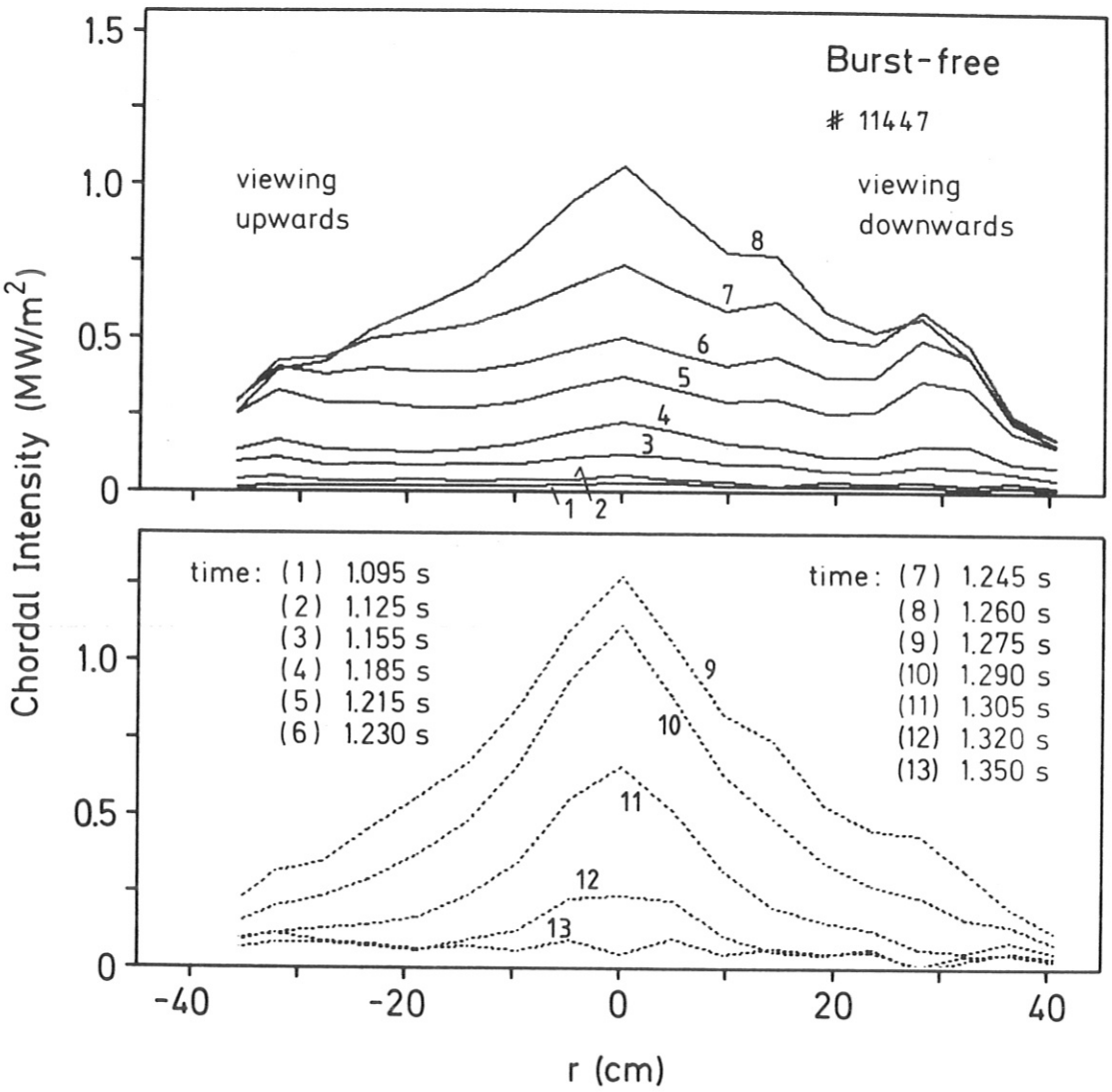

Fig.9 The continuous increase of the chord-intensity profile during the long-lasting burst-free H-mode (top) until the profile falls back to the L-mode (bottom).

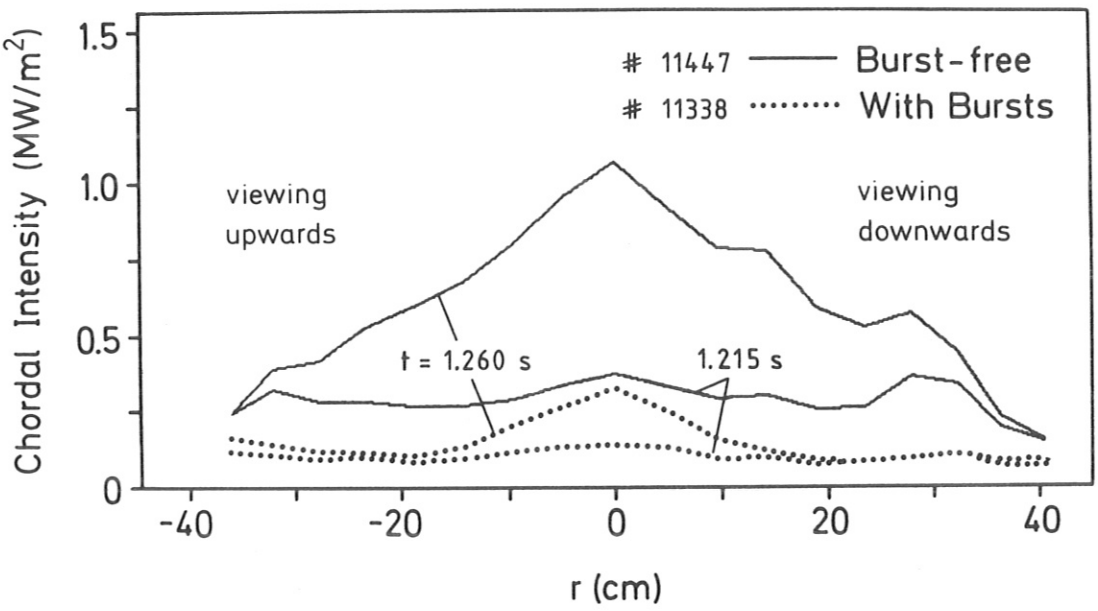

Fig.10 Comparison of the two types of H-mode discharges with regard to the chord-intensity profiles at two discrete times, shortly before each of the flat profiles starts to develop a central peak (1.215 s) and when the burst-dominated H-phase attains its maximum central chord-intensity and the absolutely burst-free H-phase terminates, respectively (1.260 s).

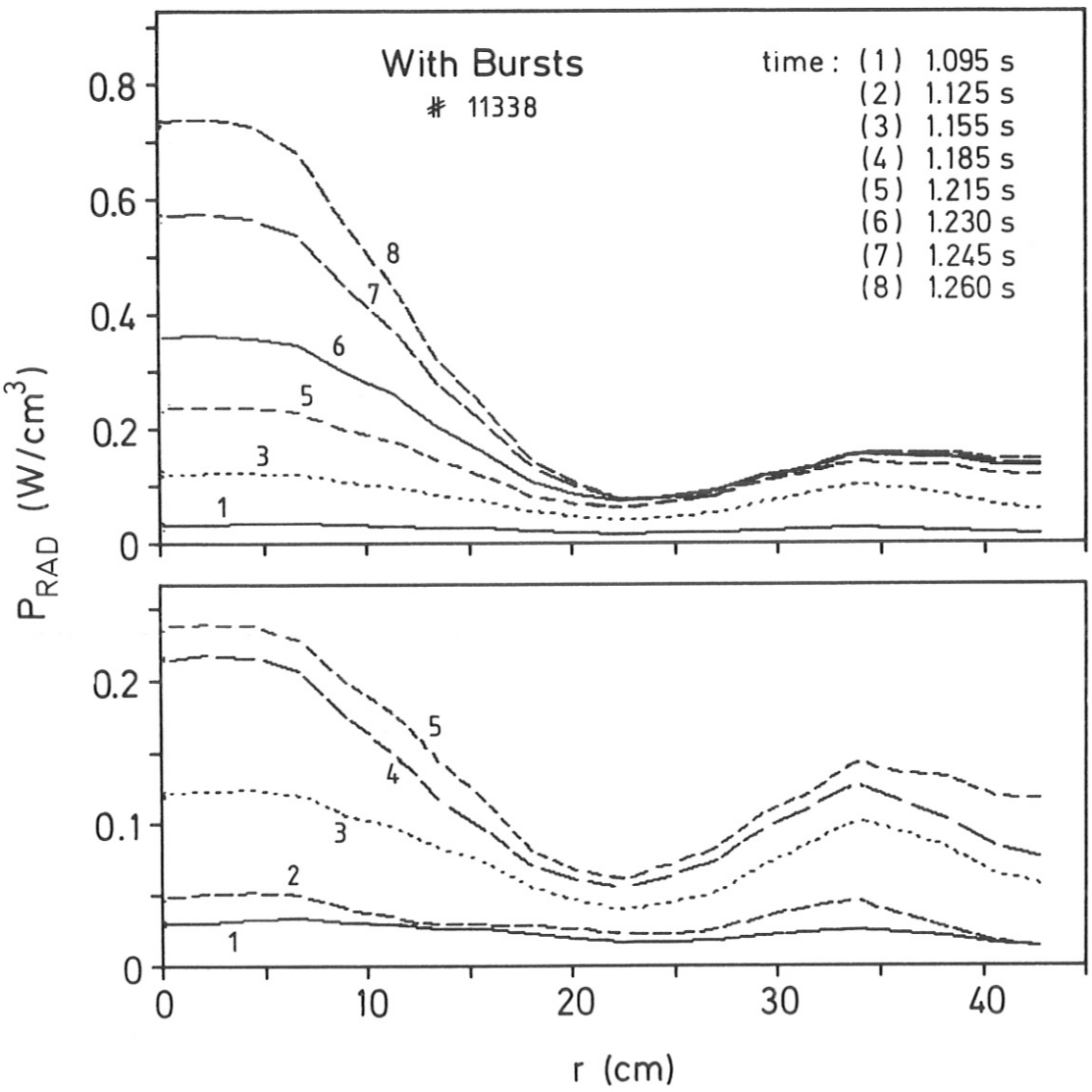

Fig.11 The radiation power density profiles of the burst-dominated H-discharge computed from the chord-intensity profiles of Fig.8 by means of Abel-inversion. Bottom: the profile evolution prior to the enhancement of central radiation density, displayed with an expanded radiation scale.

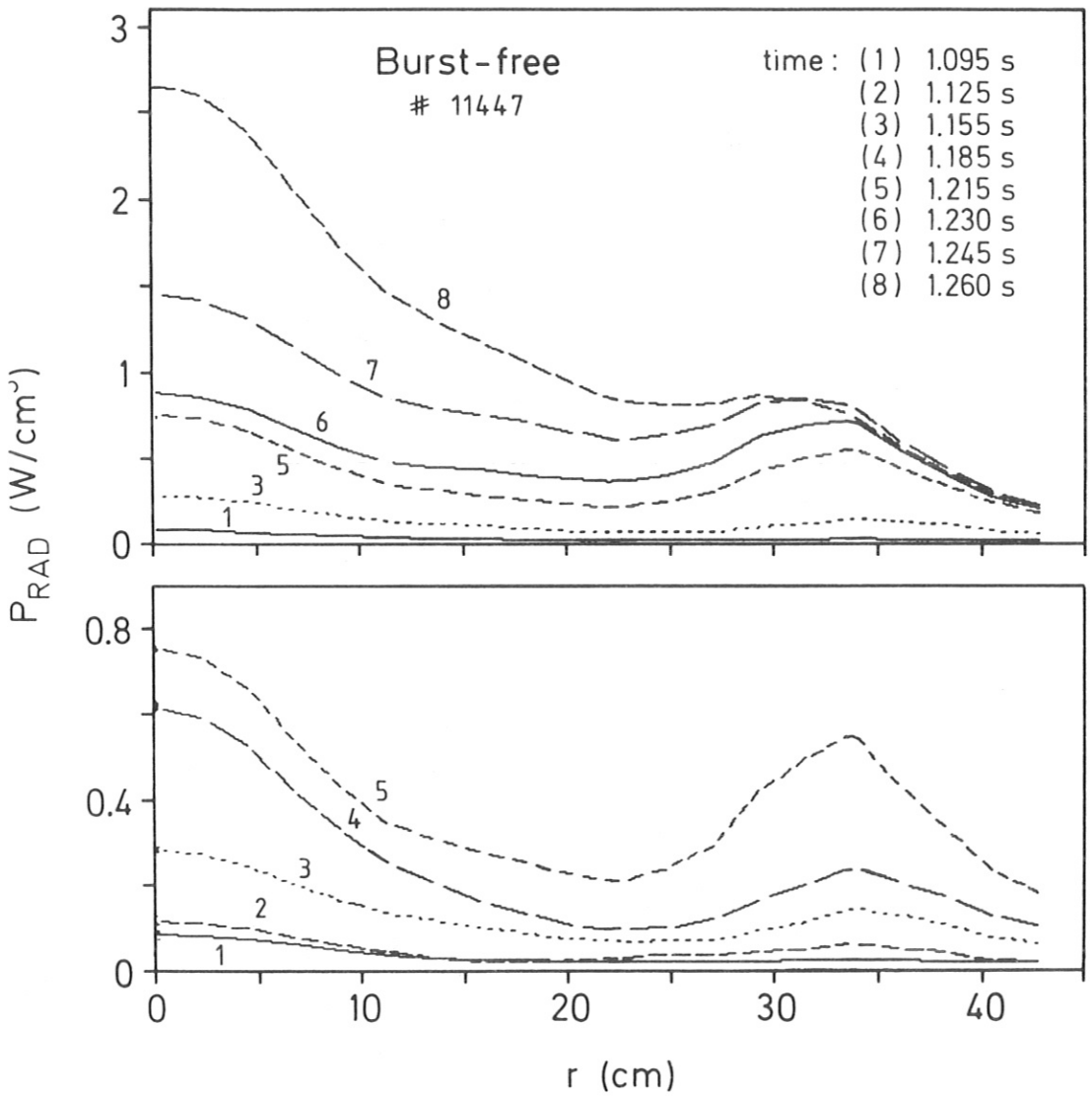

Fig.12 The radiation power density profiles of the burst-free H-discharge derived from the chord-intensity profiles of Fig.9 (for comparison, see Fig.11).

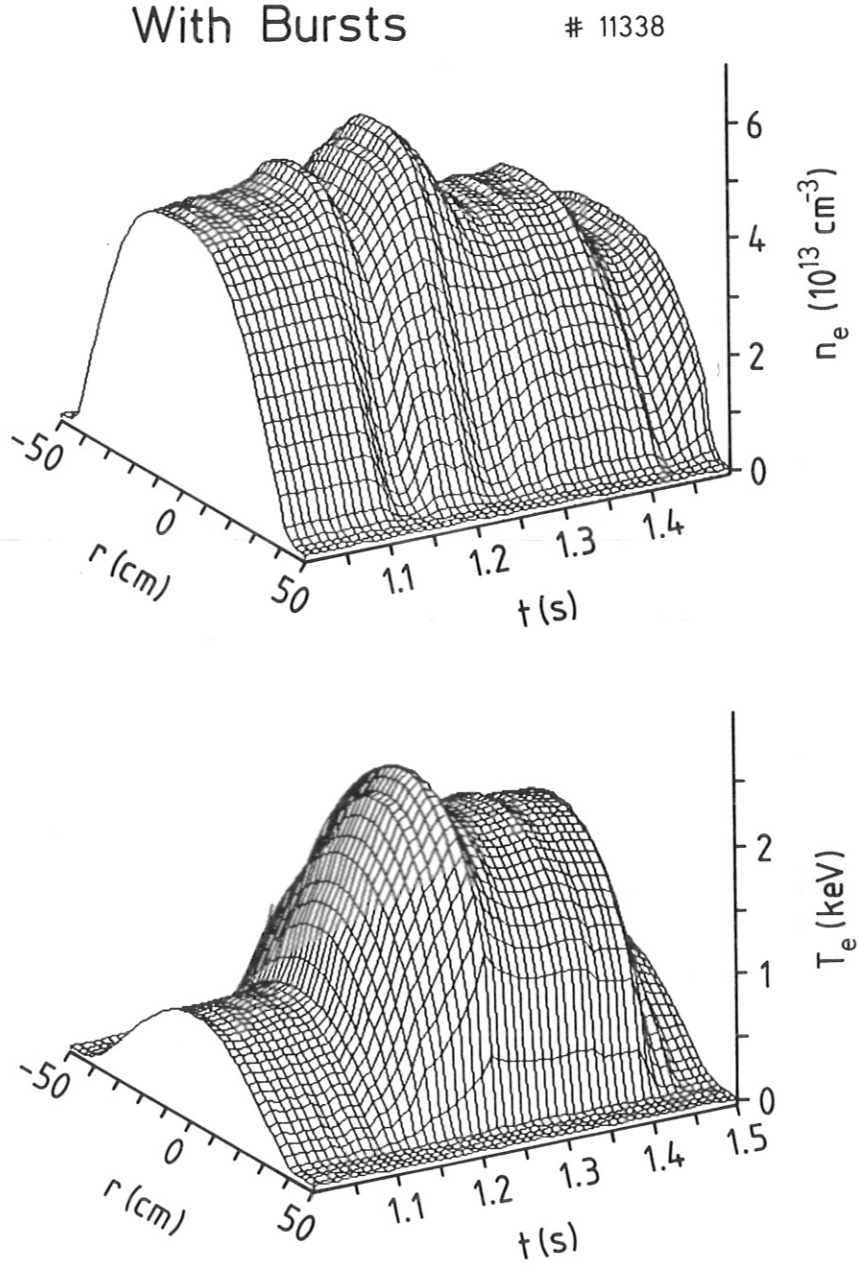

Fig.13a Time evolution of the radial plasma density and temperature profiles during the burst-dominated H-discharge.

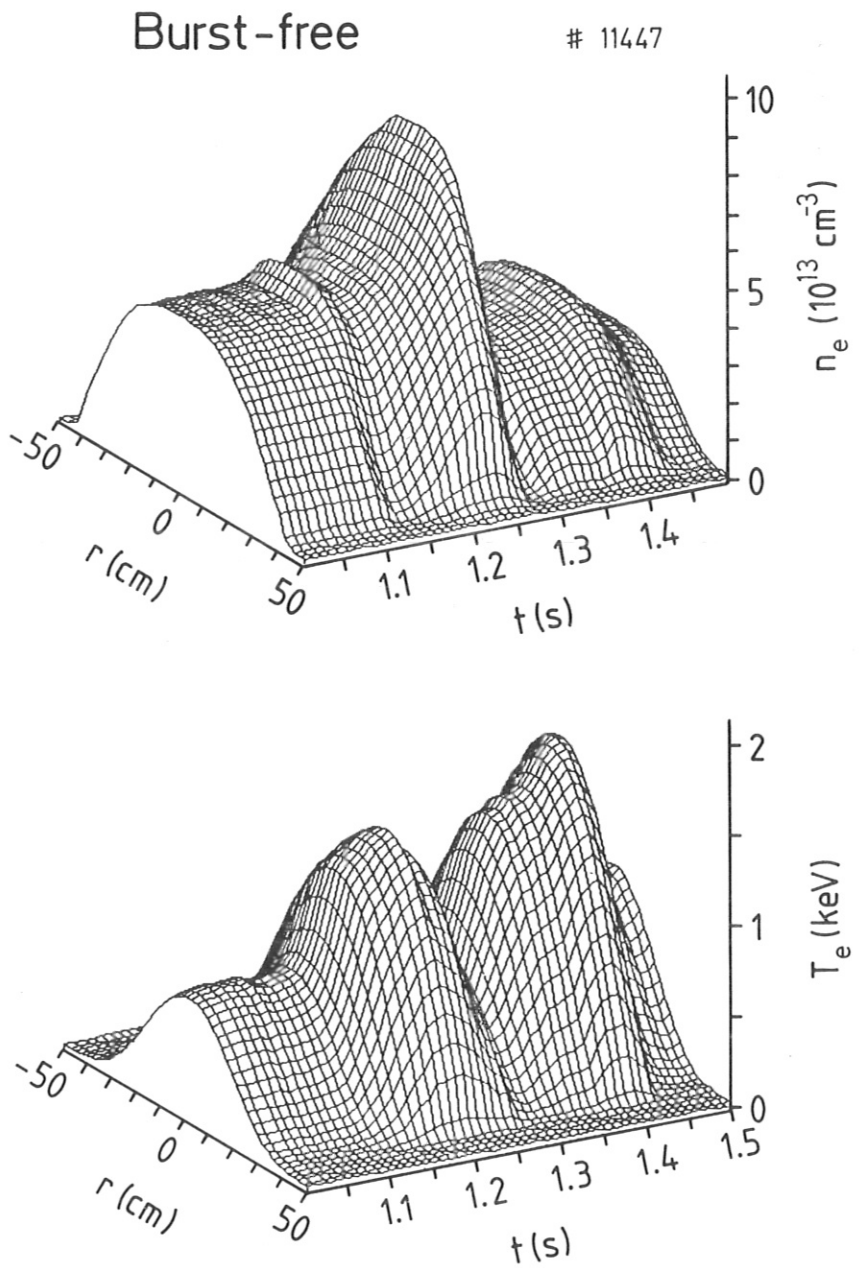

Fig.13b Time evolution of the radial plasma density and temperature profiles during the burst-free H-discharge.

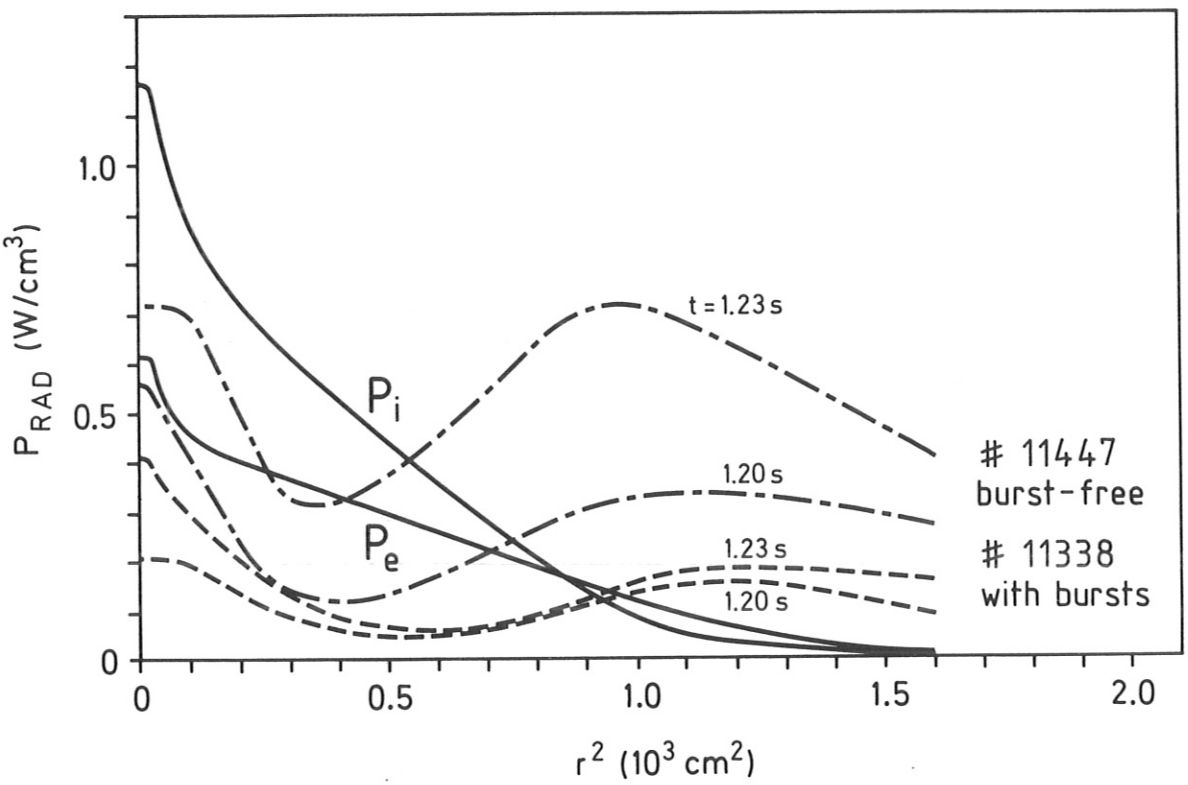

Fig.14 Radiation power density vs radius square for the two H-mode discharges introduced by Fig.5 at two instants each, shortly before and at the β maximum. Also plotted is the direct power input to the electrons (P_e) and ions (P_i) from the neutral beams.

Fig.15 (right) Plasma parameter and radiation power evolution during a burst-dominated H-discharge with low q value, high density and $D^0 \rightarrow D^+$ injection, a discharge that touches the β stability limit. (I_p = 420 kA, B_t = 2.64 T, $\bar{n}_e$ = 4.9x10^{13} cm^{-3}, $P_{OH} + P_{NI}$ = 4.1 MW, $D^0 \rightarrow D^+$; the RAD_{DIV} signal is strongly smoothed).

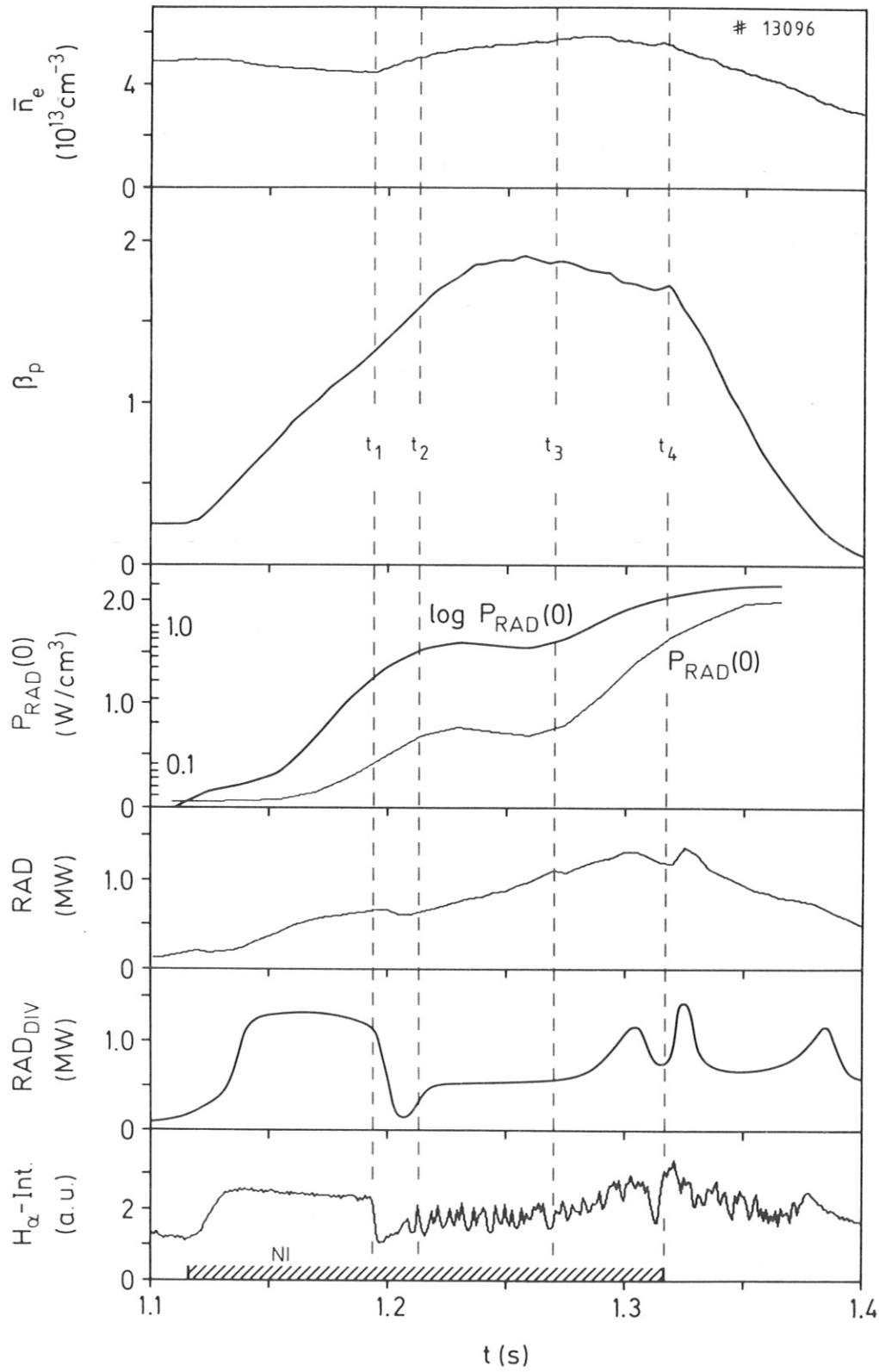
13096
$\bar{n}_e$ (10^{13}cm^{-3})
β_p
t_1 t_2 t_3 t_4
$P_{RAD}(0)$ (W/cm^3)
log $P_{RAD}(0)$
$P_{RAD}(0)$
RAD (MW)
RAD_{DIV} (MW)
H_α-Int. (a.u.)
NI
t (s)

Fig.15

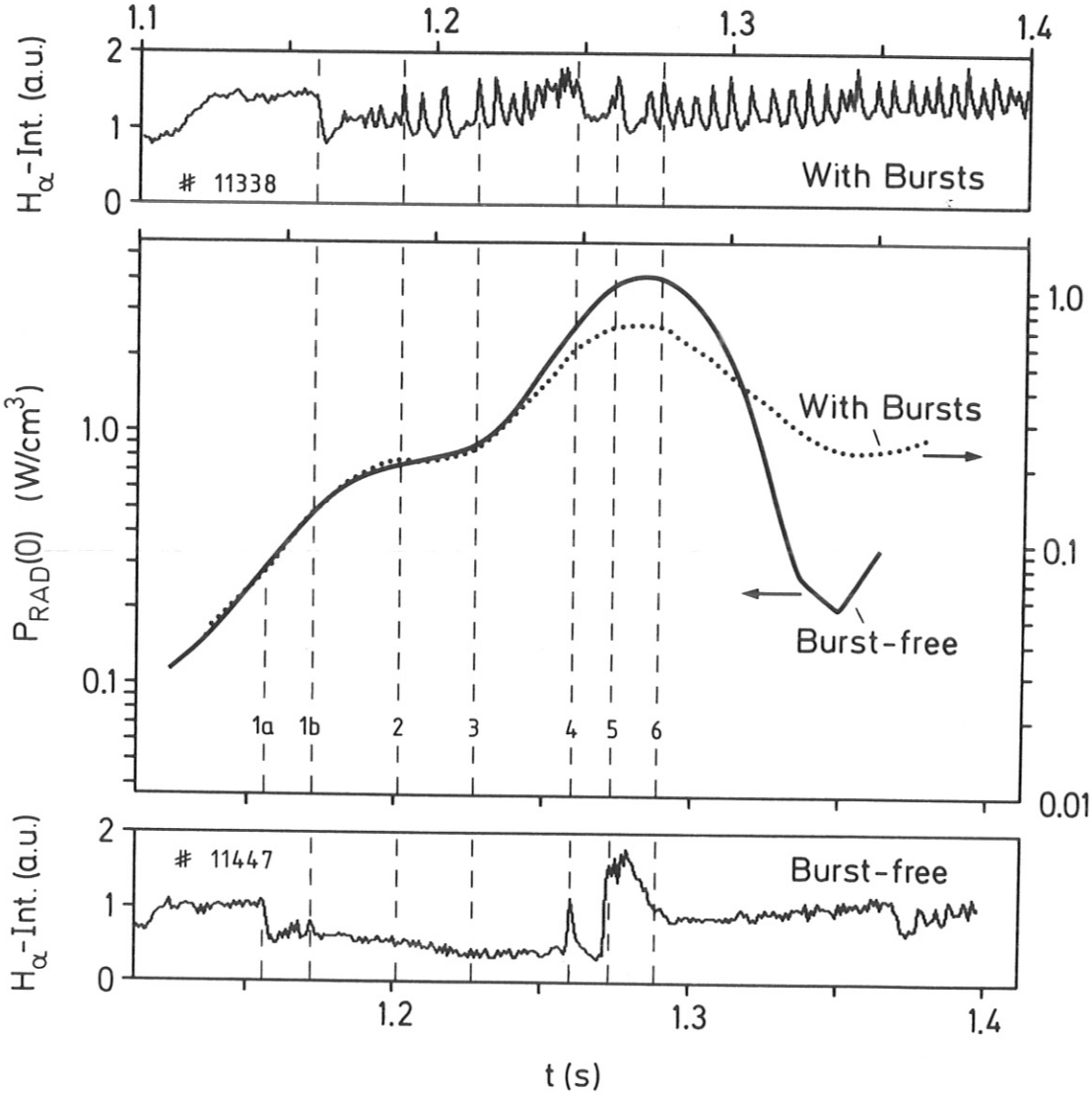

Fig.16 Dynamic behaviour of the radiation power density at the plasma centre ($P_{RAD}(0)$) for the two cases of H-mode including their prehistory. For better comparison, $P_{RAD}(0)$ is plotted logarithmically and both ordinates as well as abscissas are shifted against each other.

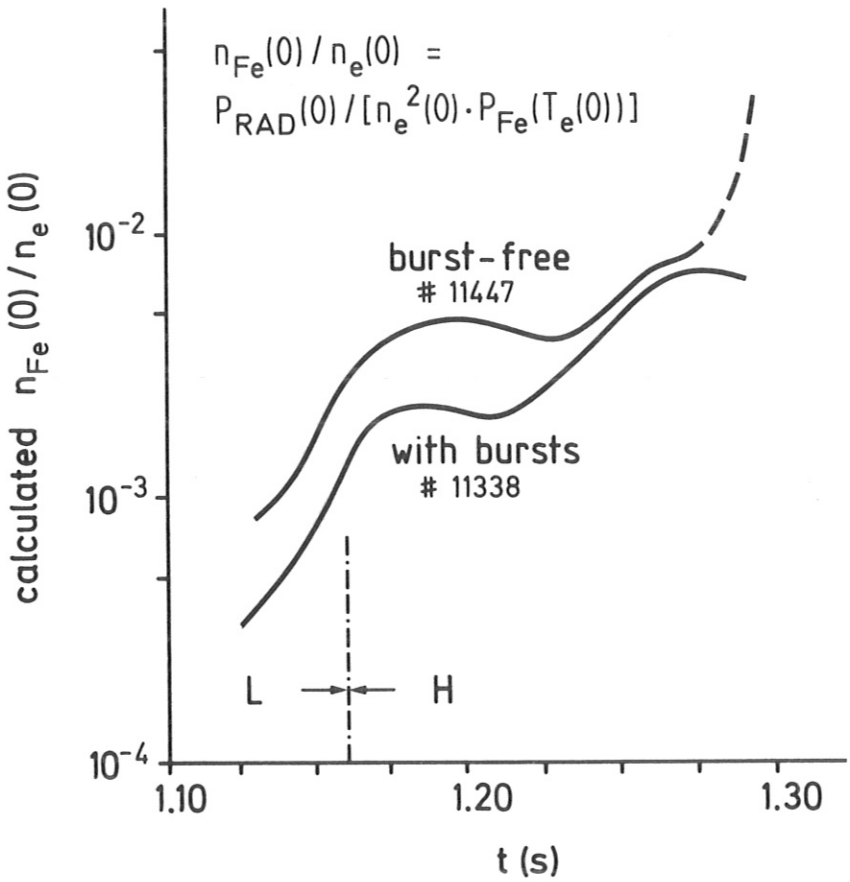

Fig.17 The calculated iron concentration at the plasma centre: the $P_{RAD}(0)$ - vs - time curves of Fig.16 are divided by the respective local plasma densities squared as well as the temperature-dependent radiative power loss function of iron ($P_{Fe}(T_e)$).

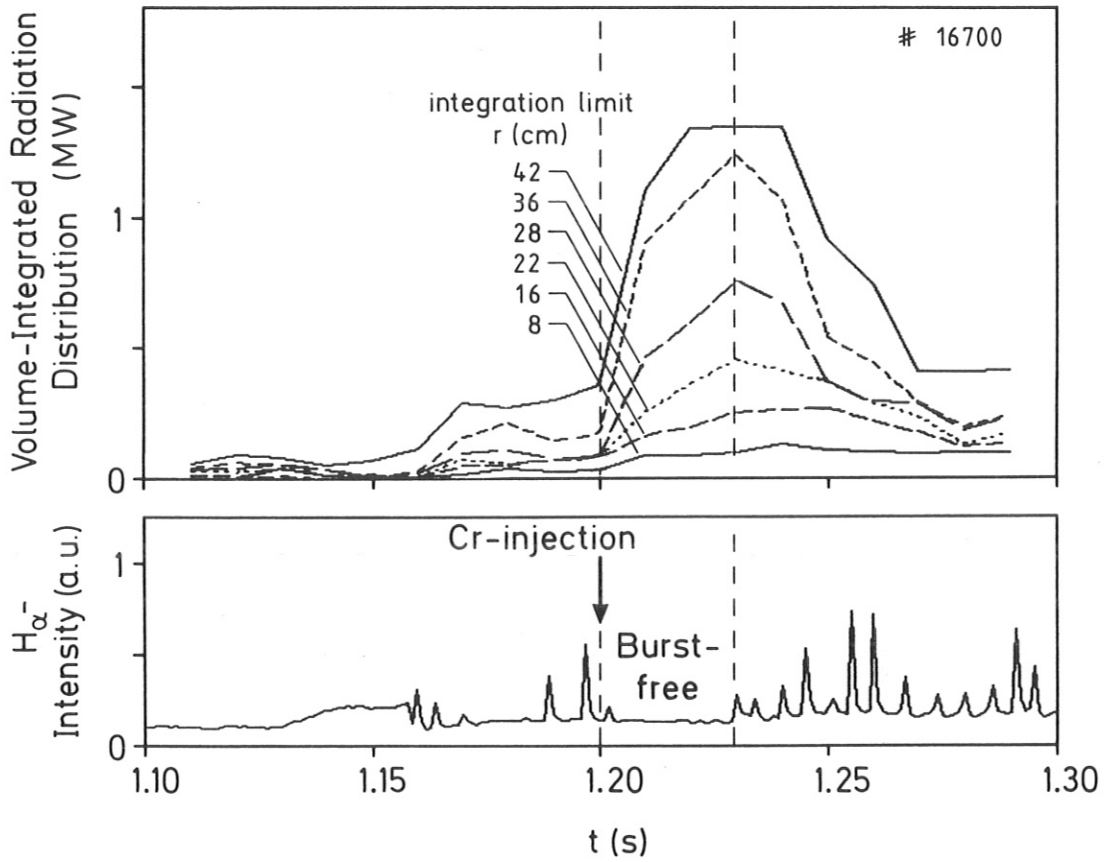

Fig.18 Time-behaviour of the radiation power integrated up to different radii when injection of chromium by laser blow-off technique abolishes the bursts in an H-discharge.

Fig.19 (right) Time history of various radiation power and impurity line-intensity signals during an H-discharge changing spontaneously from the burst-dominated into the burst-deficient phase (I_p = 320 kA, B_t = 2.17 T, $\bar{n}_e$ = 3.5 x 10^{13} cm^{-3}, $P_{OH} + P_{NI}$ = 3.3 MW, $H^0 \rightarrow D^+$, the arrows indicate the times for which profiles are given in Fig.20).

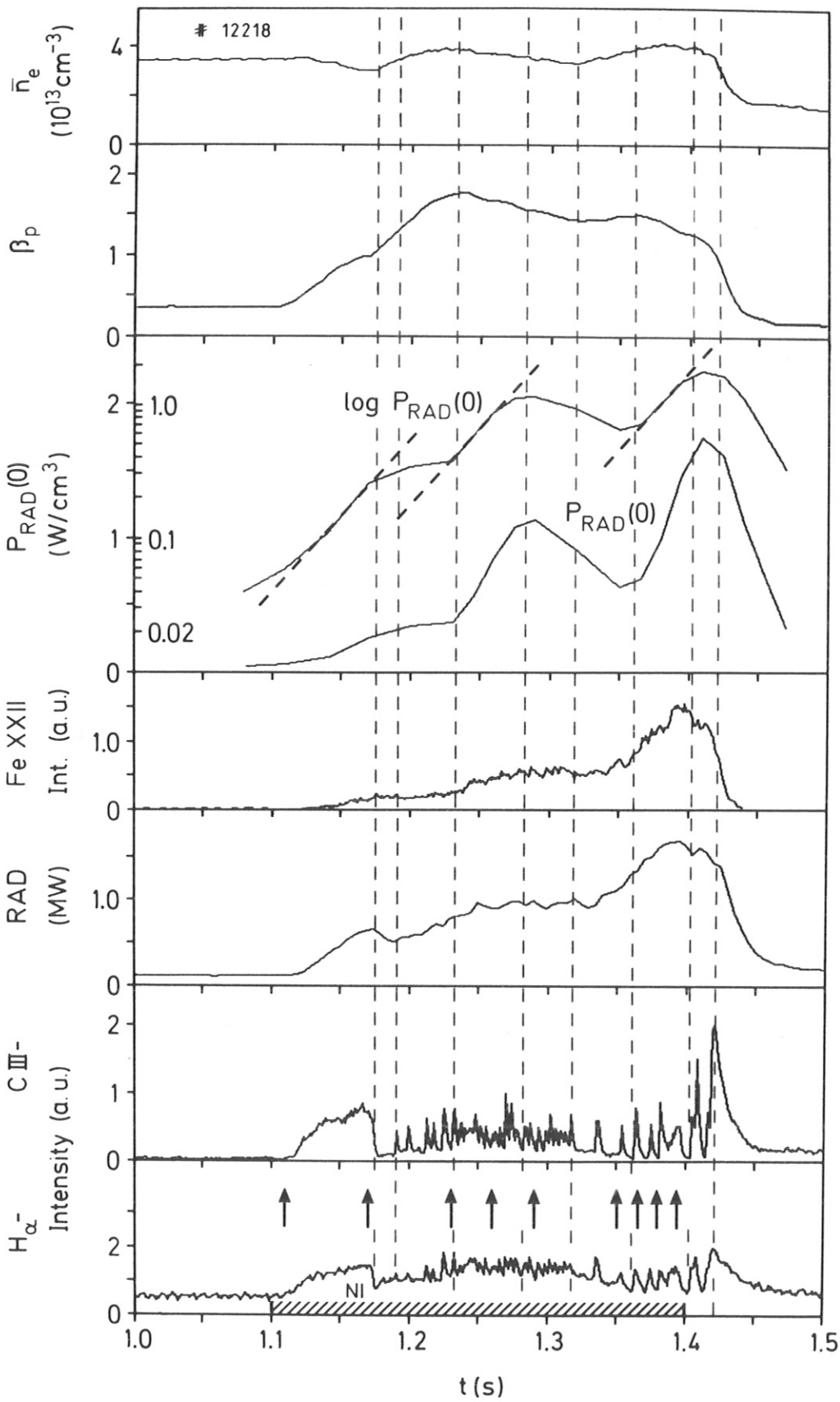
12218
$\bar{n}_e$ (10^{13}cm^{-3})
β_p
$P_{RAD}(0)$ (W/cm^3)
log $P_{RAD}(0)$
$P_{RAD}(0)$
1.0
0.1
0.02
Fe XXII Int. (a.u.)
RAD (MW)
CIII-Intensity (a.u.)
H_α-
NI
t (s)

Fig.19

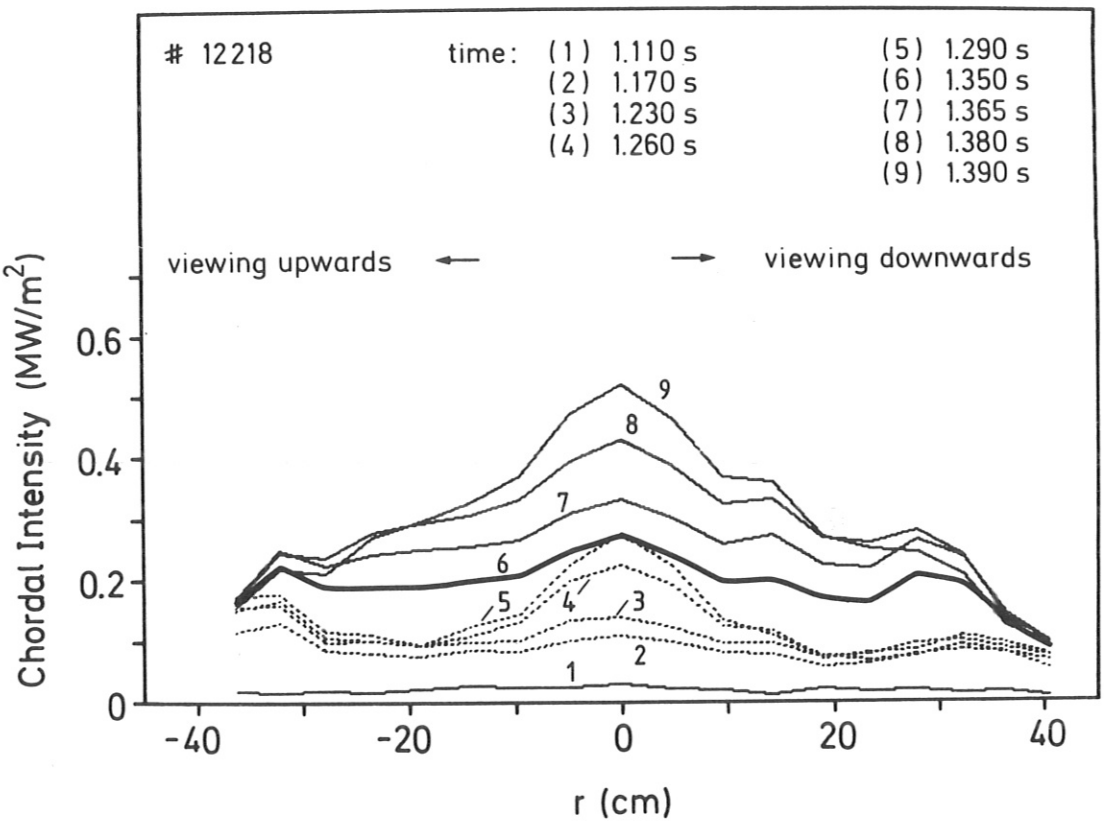

Fig.20 Evolution of the bolometric chord-intensity profile during the transition from the burst-dominated into the burst-deficient H-phase (for plasma parameters, see Fig.19).

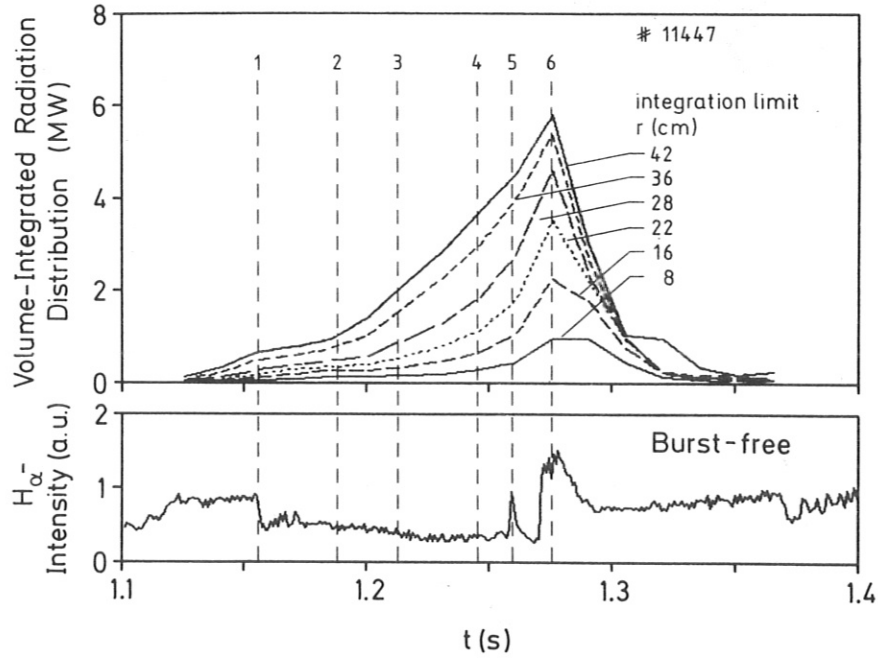

Fig.21 Comparison of the volume-integrated radiation power density, the profile of which is determined by the bolometer array, with the reading of an individual bolometer with uncollimated view in the poloidal plane for both H-mode types.

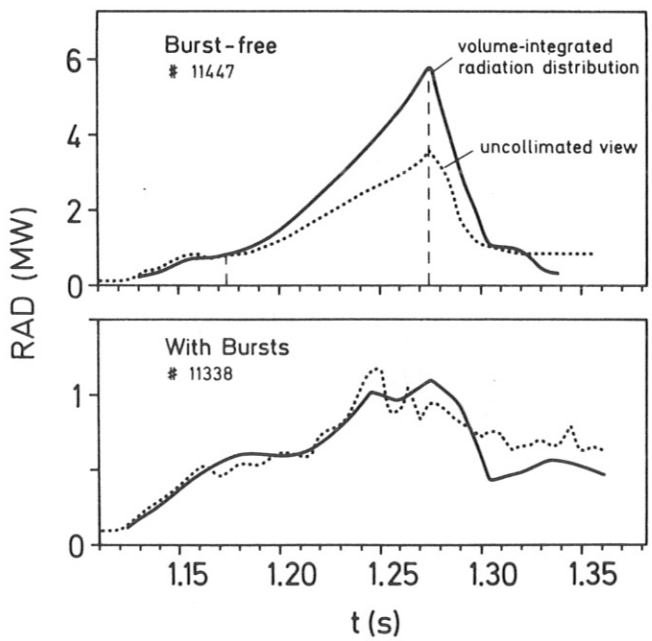

Fig.22 Different radial contributions to the volume integral of radiation power density during the burst-free H-discharge.

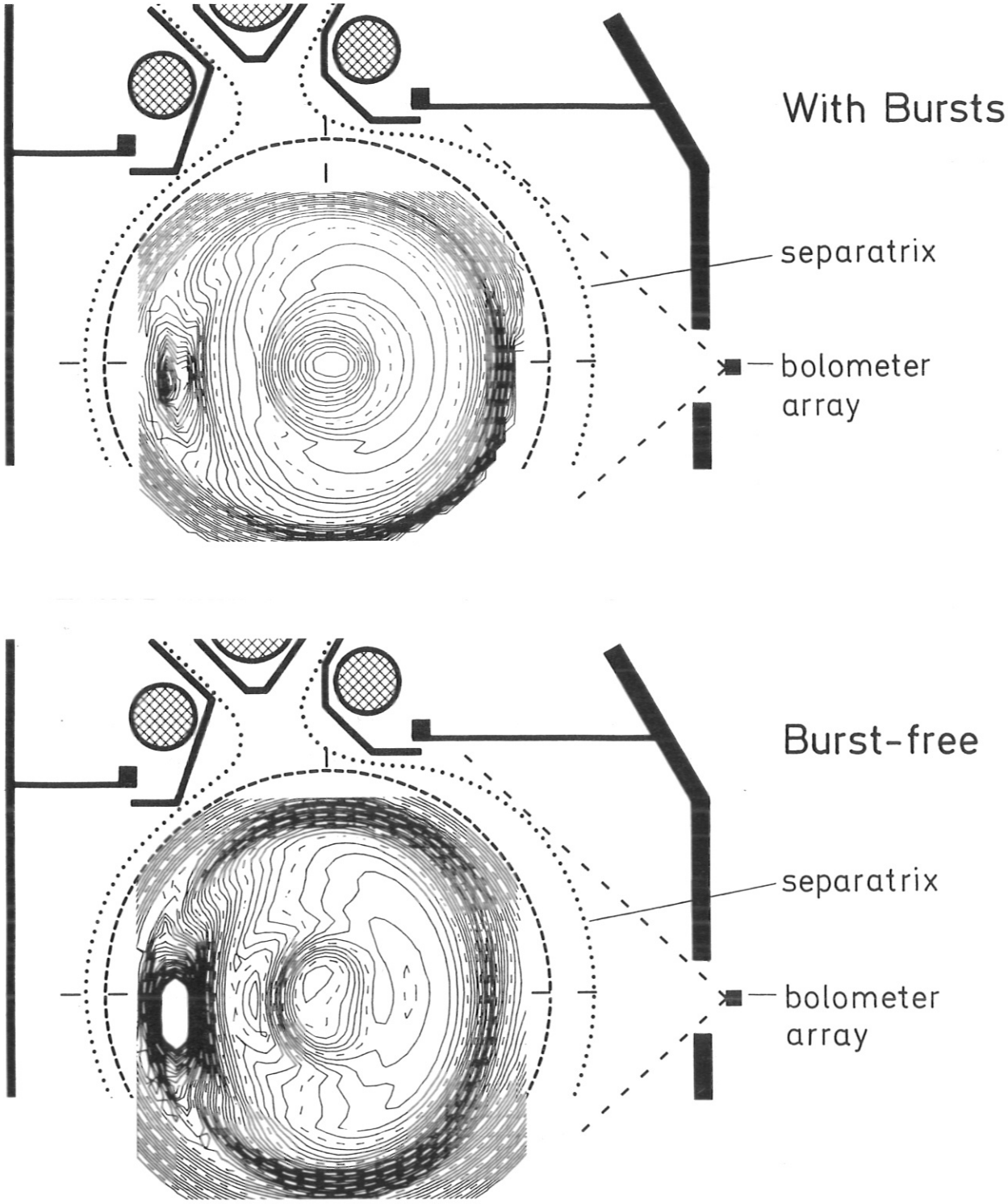

Fig.23 Typical distribution of the soft x-ray emissivity in the poloidal plane for the two kinds of H-mode, determined by two-dimensional tomography. (The distribution next to the inner wall is faulty, owing to the poor space resolution of the measurement in this region).